UNIVERSITY OF CHICAGO

A simulation-based characterization of a tagged Barium source and determination of optimal operation parameters for the capture of the released Barium ions in a radio-frequency quadrupole

A MASTERS THESIS

SUBMITTED TO THE GRADUATE SCHOOL
IN PARTIAL FULFILLMENT OF THE REQUIREMENTS

for the degree

MASTER OF SCIENCE

Field of the Physical Sciences

By

Johannes C. Eichstaedt

CHICAGO, ILLINOIS

August 2010

ABSTRACT

A simulation-based characterization of a tagged Barium source and determination of optimal operation parameters for the capture of the released Barium ions in a radio-frequency quadrupole

Johannes C. Eichstaedt

A new radionuclide-driven ^{136}Barium source allows for the tagged release of small quantities (to the order of hundreds per second) of Ba ions. This source has been developed as part of the R&D efforts for a ton-scale extension to the Enriched Xenon Observatory (EXO) experiment. The Savard group at Argonne National Laboratories (ANL) plans to experimentally characterize the source using an available radio-frequency quadrupole (RFQ) trap. This analysis seeks to determine optimal operation parameters for the RFQ and provide predictions of Ba ion energies and RFQ capture efficiencies to inform the experiment and to provide simulation results to which the experimental results can be compared. The nuclear decay reaction of the ^{148}Gd radionuclide and the recoil interactions of its daughter product ^{144}Sm with a BaF_2 Ba source layer have been simulated using SRIM. For

a BaF_2 source thickness of 500 Å the simulation predicts that 0.44 Ba ions will be knocked out for every detected Gd decay; the mean energy of the Ba ions being released has been found to be 305 ($\pm$12) eV with a median Ba ion energy of 24 eV. Using the SRIM-simulated energy and angular profile, the SIMION simulations suggest an optimal RFQ configuration: a potential well depth $U_{DC} = -20\ V$, RF parameters of $V_{RF-pp} = 450\ V$ and $\omega_{RF} = 708.6\ kHz$ with a He buffer gas pressure of $10^{-2}\ Torr$; the source mounted on a plate 1.4 mm in front of the entrance of the RFQ with the plate held at $U_{source} = 10\ V$. The simulations predict an overall capture efficiency of 46% ($\pm$2%) of all Barium ions leaving the source, with the capture efficiency being highest for low Barium exit energies and falling off rapidly for Ba energies above 40 eV.

Acknowledgements

Guy Savard has truly been generous beyond all expectation with his time and support in the process of writing this thesis at a time when the final construction of CARIBU puts a high premium on his time and attention. The graduate students Matthew Sternberg and Jonathon Van Schelt provided invaluable insights and advice. The summer student Nick Macsai has kindly assisted with the editing of the final thesis draft. The exquisite software products SRIM (James F. Ziegler) and SIMION (Scientific Instrument Services) have been most helpful for the simulations carried out in this thesis.

An implicit expression of gratitude has to go to my parents who continue to kindly support (and largely fund) my international endeavors.

Contents

List of Tables

0.1. Introduction

In different branches of experimental physics, the ability to deliver specific heavy isotopes with an ion by ion "tag" to warn the experiment of the new ion being delivered can prove invaluable for developing and calibrating ultrasensitive ion detection and manipulation techniques. This thesis presents an analysis intended to prepare the experimental characterization of such a new source which employs radionuclide decay to release a specific heavy ion from a thin layer of a target element which has been coated onto the radionuclide [**13**].

The original impetus for the development of such a source stems from the need for the ability to release single Barium ions in liquid Xenon the context of the Enriched Xenon Observatory (EXO) [**3, 15**] whose collaborators have provided the source at hand. EXO searches for the neutrinoless double-beta decay of ^{136}Xe which would provide experimental evidence for the Majorana [**4, 5, 6**] nature of neutrinos, or the lack thereof, which would place a new upper limit on a Majorana neutrino mass [**7**]). The double-beta-decay-product of ^{136}Xe is ^{136}Ba, the same isotope which forms the target isotope in the source at hand where it is present as BaF_2. As the double-beta decay is a second-order process and very rare, large amounts of the liquid ^{136}Xe are needed to detect these events and the experimental setup requires components and an environment of extraordinary radiopurity. EXO currently is operating in the form of EXO-200 which uses 200 kg of ^{136}Xe and tries to detect double-beta decay via the observation of both ionization and fluorescence in the

liquid. EXO-200 has recently been relocated to the DOE's Waste Isolation Pilot Plant (WIPP) mine 2,150 ft underground to minimize the radiation background [**10**] for its physics run.

EXO and many other double-beta-decay experiments are looking at upgrades to increase their sensitivity to a Majorana neutrino mass and in all cases this implies running with a higher exposure, essentially running with a much larger sample. The typical figure of merit being aimed at is of the order of tens of ton-years of exposure. It is proposed to extend EXO to a detector that uses liquid ^{136}Xe in a quantity of the order of one to ten tons with an associated predicted cost of in excess of $100M. The sensitivity with which the mass of the neutrino could be observed is proportional to $\frac{1}{\sqrt[2]{\text{detected counts}}}$ if no background is present, but is only proportional to $\frac{1}{\sqrt[4]{\text{detected counts}}}$ if background cannot be eliminated [**18**]. To take full advantage of the gain in exposure, all experiments must therefore also reduce background significantly. In order to do this, EXO will incorporate decay tagging to the larger full scale detector being planned.

A double-beta-decay event of ^{136}Xe would leave behind a charged ^{136}Ba isotope in the liquid xenon, whereas a neutron or background radiation would not. To require a Ba isotope to be present at the detected location of the decay event would effectively completely reduce the background of false event counts (the remaining background to neutrinoless-double-beta decay, the two-neutrino-double-beta decay, is effectively separated by the energy resolution already demonstrated by EXO-200) [**15**]. The feasibility and allocation of resources for the construction of

an extremely expensive ton-scale EXO experiment thus critically depends on the proven ability to control the background which amounts to the proven ability to extract single Ba ions from a position within the liquid Xenon. A vigorous R&D program by the Stanford group and other EXO collaborators has been ongoing for a number of years to demonstrate tagging but these efforts are hampered by the inability to test the experimental steps in a realistic and controlled fashion. The development of the source to be characterized in this thesis started in an effort to deliver Ba ions in a controlled fashion inside liquid xenon. Ideally, a source to test the extraction procedure would also be required to give a way to track how many single Ba isotopes can be expected to have been released into the liquid Xenon with high accuracy. Not only does the source at hand allow for the latter through the "tagging" of a nuclear decay in the source and the associated Barium release by the detection of the recoiling α-particle, but it also is of the right design to operate submerged in liquid ^{136}Xe without contaminating it.

Such a source would also find broader applicability in the ion manipulation field. For example, the Savard group at Argonne has developed devices called gas catchers which are used to cool recoils ions and turn them into a low-energy beam with good ion-optical properties. They are building such devices for various groups around the world for radioactive beam facilities and the detection of rare isotopes such as new superheavy elements. The Barium source that will be studied in this work could be easily adapted to produce other isotopes and be used for absolute efficiency and extraction time measurements on these gas catcher, a task which is

extremely difficult at present [**2**]. In addition, the amount of the target element needed is dramatically reduced compared to other source technologies; a layer a few nm thick over a few square millimeters suffices. The need for much reduced quantities of the target isotope can go a long way to render experiments with very rare elements feasible. For example, a sample of the rare isotope ^{120}Tellurium was needed at the CPT mass spectrometer at Argonne National Laboratories (ANL) to determine the Q-value of its double-beta decay [**12**] for the CUORICINO experiment [**8, 9**]. The isotope is only about 0.09% abundant in natural sources and a sample of it enriched to 55% was priced at $1700 per milligram ($1.7M per gram). A source technology which only requires a fraction of a microgram of the isotope will be of obvious interest to any workgroup working with such isotopes. Furthermore, the radionuclide-driven release allows for a minimalist and comparatively simple-to-operate design which would allow such a source to operate in the cleanest of environments.

The applications and advantages of such a source are numerous and an initial source has been prepared at Stanford and shipped to Argonne for characterization. The analysis presented in the following is intended to prepare the experimental characterization of the aforementioned Barium source in a setup in which the Barium ions are released in the entrance area of a radio-frequency quadrupole (RFQ) in which they can be trapped and cooled through their energy exchange with a buffer gas such as Helium at pressures to the order of 10^{-2} Torr, or 1.3 10^{-2} mbar. The setup is intended to be incorporated into the CAlifornium Rare

Isotope Breeder Upgrade (CARIBU) beam line which would allow for a transport of the Barium ions to the Canadian Penning Trap (CPT) and make a range of diagnostics available [**2**]. These would allow for precise determination and energy characterization of the released recoils, partly on the basis of and in comparison to the results of the simulations carried out in this analysis.

The first chapter of this analysis will introduce the source and the nuclear decay reaction which provides the daughter nucleus that knocks the Ba ions out of the BaF_2 layer. The second and third chapters will introduce the nuclear interaction software suite "the Stopping and Range of Ions in Matter" (SRIM) and present simulation results of the nuclear interactions within the Barium source including the expected angular and energy profiles of Ba ions exiting the source. The fourth and fifths chapters will introduce the theory of RFQs and the SIMION software used to model the interactions of the charged Ba ions with the buffer gas and the electric fields in the RFQ. In chapter six, in SIMION-simulations of the RFQ, different operation parameters of the RFQ are examined in their effect on the overall efficiency of Barium ion capture from the source; the simulations use the knowledge gained through SRIM of the angular and energy profiles of the Barium ions as they exit the source. It is attempted to determine a set of RFQ operating parameters (a "suggested RFQ configuration") which maximizes the RFQ's Ba ion capture efficiency given the Ba source at hand. Chapter seven assumes this recommended configuration and presents simulation results about capture performance for the

source Ba energy spectrum, as well as for Ba entering the RFQ at different Ba angles and energies in general.

CHAPTER 1

The Barium Source

1.1. Tagged Barium Emission

The source was provided by Maria Montero Díez, a Stanford member of the EXO collaboration. 25 μl of a solution of $^{148}_{64}Gd(NO_3)_3$ in isopropanol is electroplated on a surface barrier detector. Then a thin layer of BaF_2 is vapor-deposited on top, in our case the BaF_2 has a thickness of 500 Å [**18**]. This Gadolinium isotope has a half-life of 74.6 years [**17**]; it decays at a rate of 106 Becquerel. Its only known decay channel is α-decay, its daughter nucleus ^{144}Sm is stable. Figure 1.1 depicts the source schematically. The α-particle that is being released is to

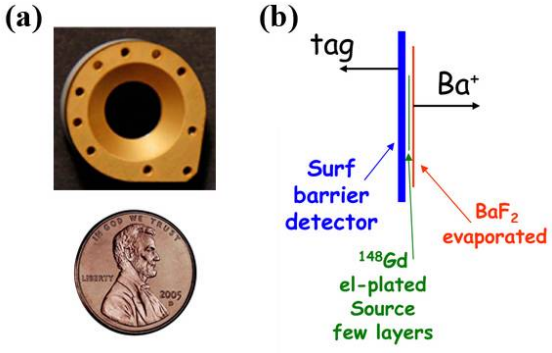

Figure 1.1. (a) Ba+ source with penny for scale (b) schematic drawing of the source (BaF_2 in the source has a thickness of 50nm.) Adopted from [**18**].

be detected by the surface barrier detector if it leaves the radionuclide layer in the direction of the detector. Conservation of linear momentum demands that the ^{144}Sm daughter nucleus will exit the $^{148}_{64}Gd(NO_3)_3$ layer in the opposite direction towards the BaF_2 layer, where it is expected to knock out Barium ions (as well as some Fluorine) with a certain probability. The Barium in the BaF_2 layer is ^{136}Ba, the same isotope that is created in the double-beta decay of ^{136}Xe. Among other quantities the relative probability that a Ba ion will be knocked out in the forward direction as a consequence of the Gadolinium decaying into Samarium will be the object of this analysis. This configuration effectively provides a time-stamp for the nuclear decay event ("tagging") which can be related to the probability of Barium release by the source at that moment in time, a unique trait for this source technology that makes it so attractive for use in a planned ton-scale EXO experiment. As half of the decays release their products in the opposite directions such that no Barium is released from the source and no α-particle is detected, the above decay rate of 106 Becquerel is effectively reduced to half.

The Fluoride knocked out of the BaF_2 and the Samarium which might penetrate the BaF_2 layer and escape the source will be addressed in the following two chapters, however it will not further be considered in the RFQ simulations. Should Samarium ions be trapped in the RFQ - which is conceivable given the recommended RFQ configuration - the diagnostics available in the CARIBU beamline would be able to identify these ions. The 3 MeV α-particles released towards the

El	**A**	**Z**	**N**	Atomic Mass (u)	(±)
Gd	148	64	84	147.918115	0.000003
Sm	144	62	82	143.911999	0.000003
Ba	136	56	80	135.9045759	0.0000004
F	19	9	10	18.99840322	0.00000007

Table 1.1. AME03 data for relevant isotopes.

BaF_2 layer are exceedingly unlikely to knock out a much heavier Barium ion and are neglected in the further analysis

Table 1.1 summarizes the atomic masses of the relevant isotopes according to the 2003 Atomic Mass Evaluation Update [**1**].

1.2. Calculation of Decay Energies

Based on the AME03 isotope masses the decay ^{148}Gd $\rightarrow$ ^{144}Sm + ^{4}He has an associated Q-value of

$$Q = 3.27 \text{ MeV} \tag{1.1}$$

Conservation of linear momentum demands that $p_{He} = p_{Sm}$. In the center of mass frame of the Gd nucleus relativistic conservation of energy demands that

$$m_{Gd}c^2 = \sqrt{m_{Sm}^2c^4 + (p_{Sm}c)^2} + \sqrt{m_{He}^2c^4 + (p_{He}c)^2} \tag{1.2}$$

which in combination with the constraint on the momenta implies that $p_{He} = p_{Sm} = 154.08$ MeV/c. The kinetic energies of the isotopes follow from

$$T = \sqrt{m^2c^4 + (pc)^2} - mc^2 \tag{1.3}$$

as

$$T_{Sm} = 88.56 \text{ keV} \qquad T_{He} = 3182.65 \text{ keV} \tag{1.4}$$

such that the Sm and He split the Q-value about 1:36 which is in inverse proportion to their masses. For the given Q-value, a non-relativistic calculation of their kinetic energies would differ by less than 1/1000.

CHAPTER 2

SRIM Simulations of the atomic Processes in the Barium-Source

2.1. SRIM Introduction

Having derived the kinetic energies of the decay products, the full atomic recoil process that ensues from the Samarium entering the BaF_2 cubic crystal structure can be simulated via a full Monte Carlo simulation. The software "the Stopping and Range of Ions in Matter" (SRIM) has been written explicitly for this purpose by J. F. Ziegler, and its powerful TRIM module ("the Transport of Ions in Matter") is particularly suited for the purpose of this analysis [**20**]. The level of detail that is simulated for every ion is described by Ziegler:

> During the collisions, the ion and atom have a screened Coulomb collision, including exchange and correlation interactions between the overlapping electron shells. The ion has long range interactions creating electron excitations and plasmons within the target. These are described by including a description of the target's collective electronic structure and interatomic bond structure when the calculation is set up (...). The charge state of the ion within the target

is described using the concept of effective charge, which includes a velocity dependent charge state and long range screening due to the collective electron sea of the target.

For heavy ions such as Samarium SRIM in its 2010 version is accurate on average in its calculation of stopping powers to within 8.1% of the experimental results, based on about 9000 data-points [**22**]. However, only few of the data-points reference experimental results with ion energies as low as the one used here and the error is likely to be larger [**21**]; only a full experimental realization will provide hard data to compare the simulations to. Figure 2.1 shows the TRIM module in the process of carrying out a Monte Carlo simulation. Shown are the atomic displacements after four Sm ions with the kinetic energy calculated above (89 keV) have penetrated 500 Å of the BaF_2 compound.

2.2. SRIM Setup

The data listed for BaF_2 in the references refers to Ba in its most abundant isotope ^{138}Ba [**19**]. As the source under analysis contains ^{136}Ba the atomic weight and the density of the compound were adjusted accordingly (from 4.89 to 4.85 $\frac{g}{cm^3}$) which is the method the authors of SRIM suggest [**20**]. Figure 2.2 shows the settings that go into the full TRIM simulation. The settings in the lower right corner of Figure 2.2 are of particular interest, they indicate displacement, lattice as well as surface binding energies in eV. Displacement energy is defined as "the energy that a recoil needs to overcome the lattice forces and to move more

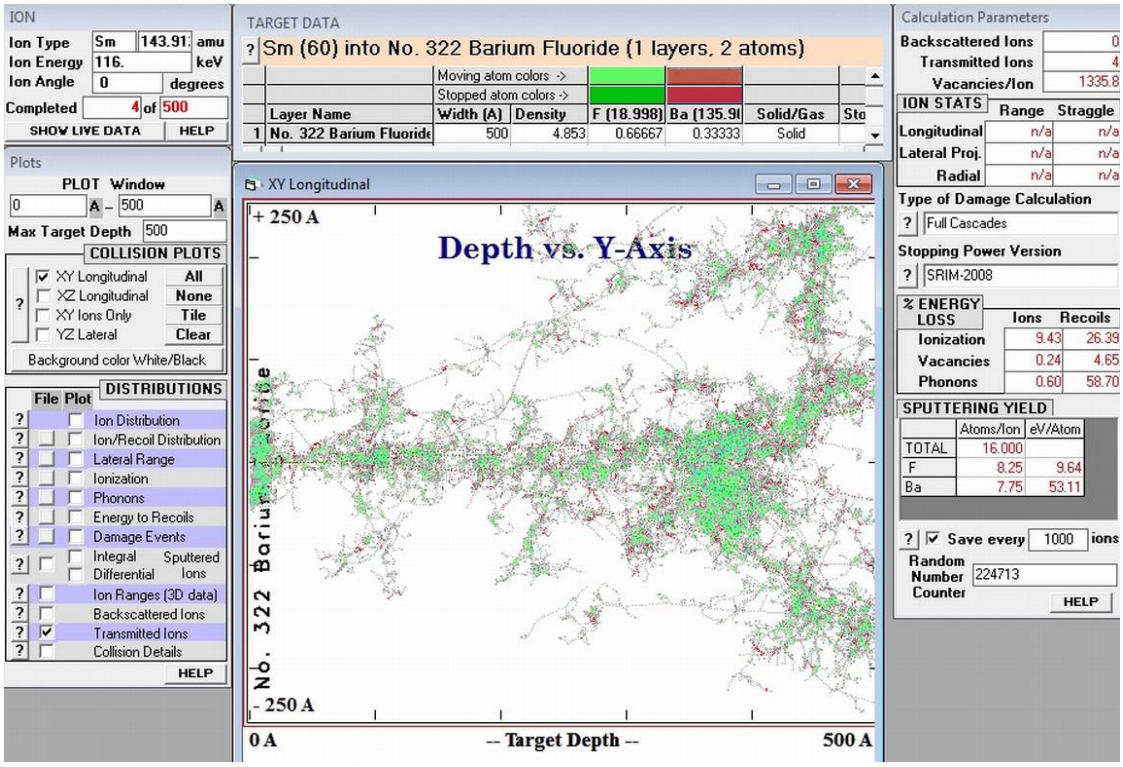

Figure 2.1. The TRIM module of the SRIM software. The plot in the middle shows the penetration of Samarium into BaF_2. The dotted lines in the middle show the places where the Sm ion had a collision, the green dots indicate Fluorine ion cascades, the red dots cascades of Barium.

than one atomic spacing away from its original site" [**20**]. Lattice binding energy indicates the amount of energy a recoiling ion loses when it does leave its lattice site. According to [**20**], the energy is presumed to go into phonons.

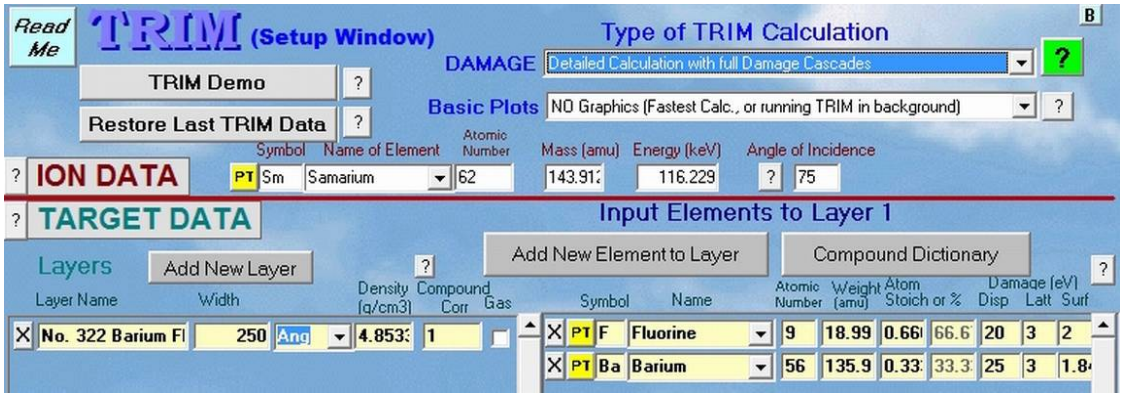

Figure 2.2. TRIM settings are shown for the full Monte Carlo simulation of the atomic processes within the Ba+ source described above.

The displacement energy (DE) is of particular relevance to our analysis, as we are interested in those Ba ions that are knocked out of the BaF_2 layer. Fortunately, typical values are established for BaF_2 which are listed in SRIM's compound dictionary [**24**]. Nevertheless, to test the sensitivity of the simulation on these assumptions simulations were carried out with 2000 incident ions each in which the DEs were varied by $\pm 20\%$, which affected the rates of ejected target and transmitted incident ions as indicated in Figure.2.3.

For Barium, a reduction of the DE by 20% from 25 to 20 eV resulted in a 3% increase in knocked out Ba ions per incident Sm ion. For Fluorine such a reduction in DE resulted in 7% more knocked out ions. For a 20% increase in DE the knock-out rates decreased by 13% and 10% respectively. It thus seems that changes in the DE in the range of the values chosen will translate into moderate changes in the ejection rates; reductions of the DE from the suggested values seems to affect

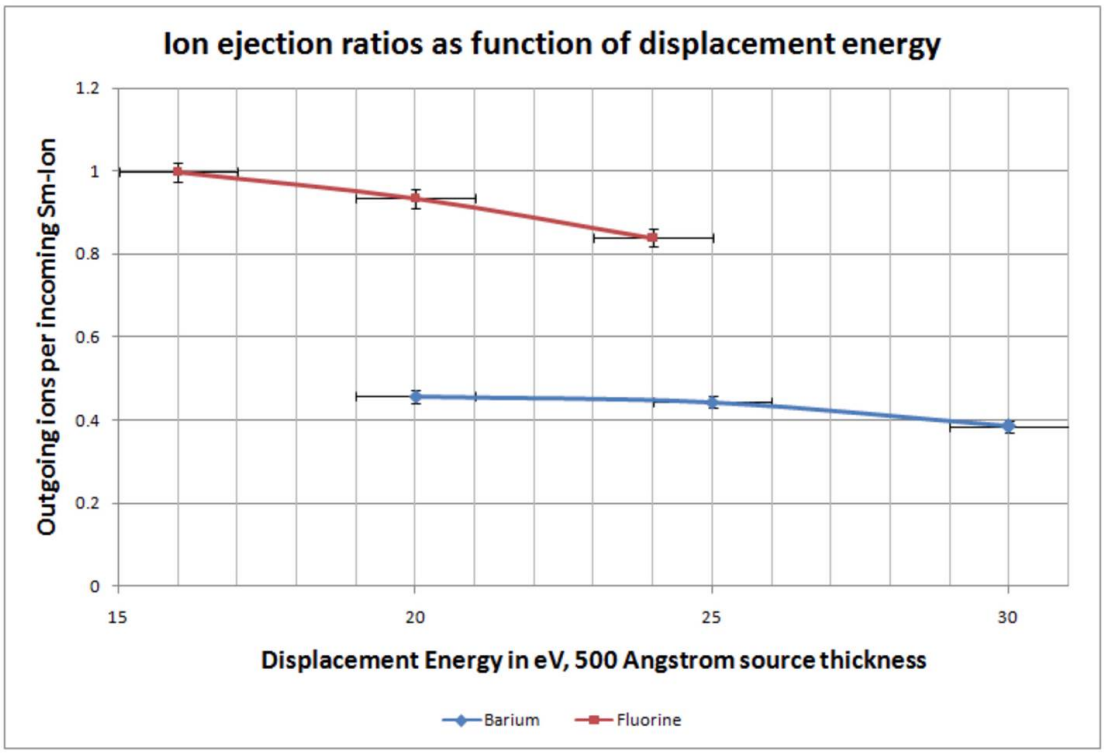

Figure 2.3. Barium (blue) and Fluorine (red) ejection rates per given incident Samarium ion on the 500 Å BaF_2 layer. The displacement energy parameter that is used by the TRIM simulation was varied $\pm 20\%$ from the recommended settings of 20 eV for Fluorine and 25 eV for Barium [**24**]. The higher the value used for the displacement energy parameter the fewer Ba/F ions are knocked out of the BaF_2 layer and vice versa. These values were obtained by averaging over 2000 incident Sm ions which were distributed in their angles-of-incidence according to the availability of solid angle for that angle of incidence. Vertical error bars at times are too small to be seen.

the ejection rates substantially less than their increase. The transmission of Sm ions through the BaF_2 was not affected by changes in this parameter.

2.3. SRIM Automation

As indicated in Figure 2.2, TRIM can only simulate one incident ion angle at a time. However, as the decay of the Gadolinium has no preferred direction the incidence of its daughter nucleus Sm on the BaF_2 is isotropic. To generate credible simulation data, the simulation was carried out for nine different incident angles which were weighted by the corresponding availability of solid angle and the results then combined into one "operational dataset". SRIM itself has very little built-in functionality to simplify this rather time-consuming task, so a series of scripts was devised to provide this and other extended functionality. As it was recognized that this toolkit would be of ongoing benefit to future users of SRIM the automation workflow was documented and the scripts were made available in the context of the thesis. This documentation can be found in the appendix.

CHAPTER 3

SRIM Results

3.1. Thickness of the BaF_2 Layer

Figure 3.1 shows a plot of knocked out Ba/F or transmitted Sm ions per incident Sm ion for different BaF_2 thicknesses. For thin layers of BaF_2 fewer F/Ba ions are knocked out, presumably because of the limited availability of ion targets both for the Sm as well as for target ions that are recoiling into the BaF_2 layer. For thicker layers both the incident Sm ions as well as the recoiling target ions are increasingly retarded by the remaining atomic layers and might not have the energy to reach the surface. The transmission of Samarium is monotonically decreasing with BaF_2 thickness, as one would expect. A maximum knock-out efficiency for Barium of 6.5 Ba ions/Sm ion seems to be reached at a BaF_2 thickness of around 100 Å ($\pm$20 Å); which also seems to be the maximum for Fluorine (12.4 F per incident Sm). Such a thickness would be recommended if one wanted to produce a highly efficient Barium source which maximizes the number of Ba ions released from the source based on the Gadolinium decay discussed above. If the source was used, for example, for the calibration of gas catchers and other parts of a heavy ion beam-line, this would be the preferred configuration. Given the 106 Becquerel estimate for the source, at this maximum ejection configuration Ba ions are predicted to

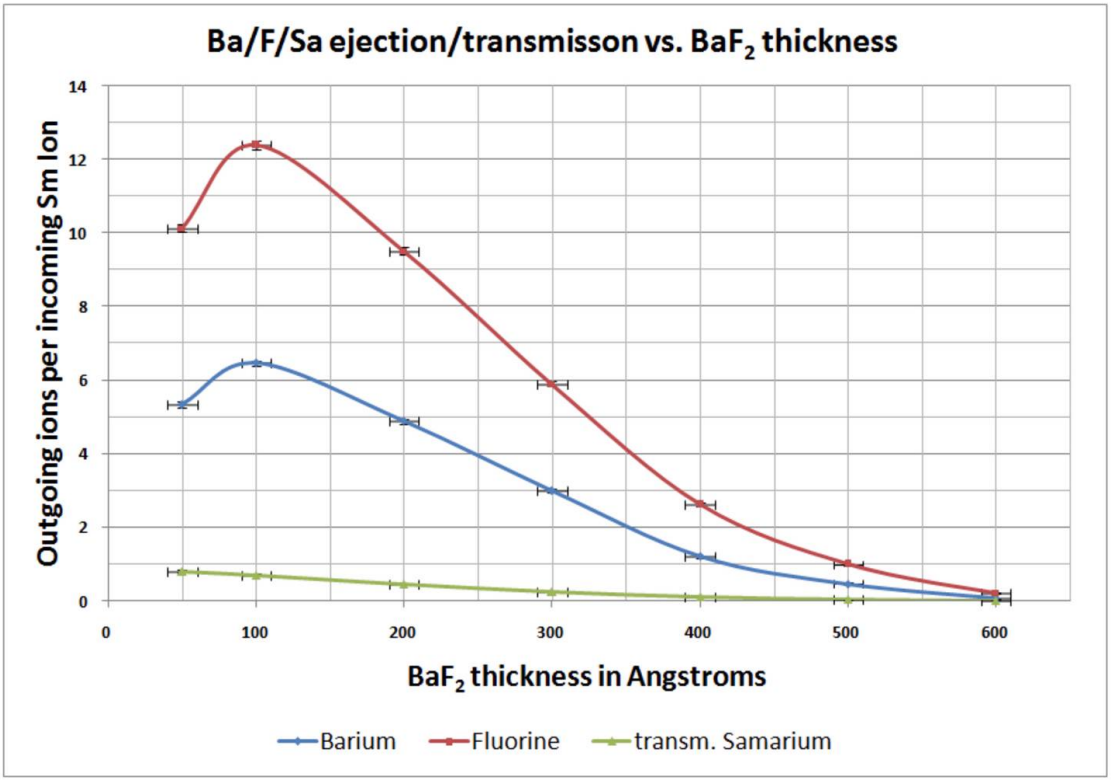

Figure 3.1. Ba/F ions knocked out per incoming Sm-ion (ejection), or fraction of Sm ion transmitted for different BaF_2 thicknesses. Every datapoint represents 5000 incident Sm ions which were averaged over and distributed in their angles-of-incidence on the BaF_2 according to the availability of solid angle for that angle of incidence. Vertical error bars are at times too small to be seen.

be emitted at a frequency of 342 Hz. The recoiling Ba ions are expected to be distributed over a few charge states (0^+, 1^+, 2^+) and to be a single ion, i.e. the molecule BaF_2 is not broken apart in the process.

The source at hand has a BaF_2 layer thickness of 500 Å. The TRIM simulation predicts that 0.44 Barium ions will be knocked out per given incident Sm ion. In

the EXO experiment the source would be preferred to emit one Ba ion on average for every tagged Gd decay [**13**], our simulation results suggest that such an emission rate could be achieved with a source of approximately 410 Å (±10 Å) thickness. In fact, at this separately simulated source thickness the predicted Ba knock-out ratio is 1.02 ± 0.02 Ba Ions per incident Sm ion. The prediction for Fluorine knock-out rates at the thickness of the source at hand is 0.99 ions per incident Sm ion, while 4.1% of the Sm ions are predicted to be transmitted through the layer. Given the estimated radioactivity of the ^{148}Gd in the source, the Ba ions are predicted to be released by the source at a rate of 23.3 (±1.6) Hz.

3.2. Angular & Energy Profiles of the released Ba Ions (500 Å Source)

Figure 3.2 shows the energy profile of the exiting Ba ions. For 30,000 incoming Sm ions on the BaF_2 layer 0.44 (± 0.03) Ba ions are knocked out for every incoming Sm ion. The overall median energy of the knocked out Barium ions is 24.1 eV. The mean energy is 305.1 (±12.3) eV; the divergence between the above two figures indicates the high skewness of the distribution. 75% of all exiting Ba ions have an energy less than 80 eV, and 90% fall below 397 eV. The remaining Ba ions have energies that extend in a long tail all the way up to 34.5 keV.

The angular profile (Figure 3.3) shows a sinusoidal peak at 45 °. Ba ion trajectories within the BaF_2 with high angles from the normal - that is Ba ions which are largely parallel to the exit surface - have to cover a much increased range in the BaF_2 layer and thus the count of Ba ions leaving at such high angles from the

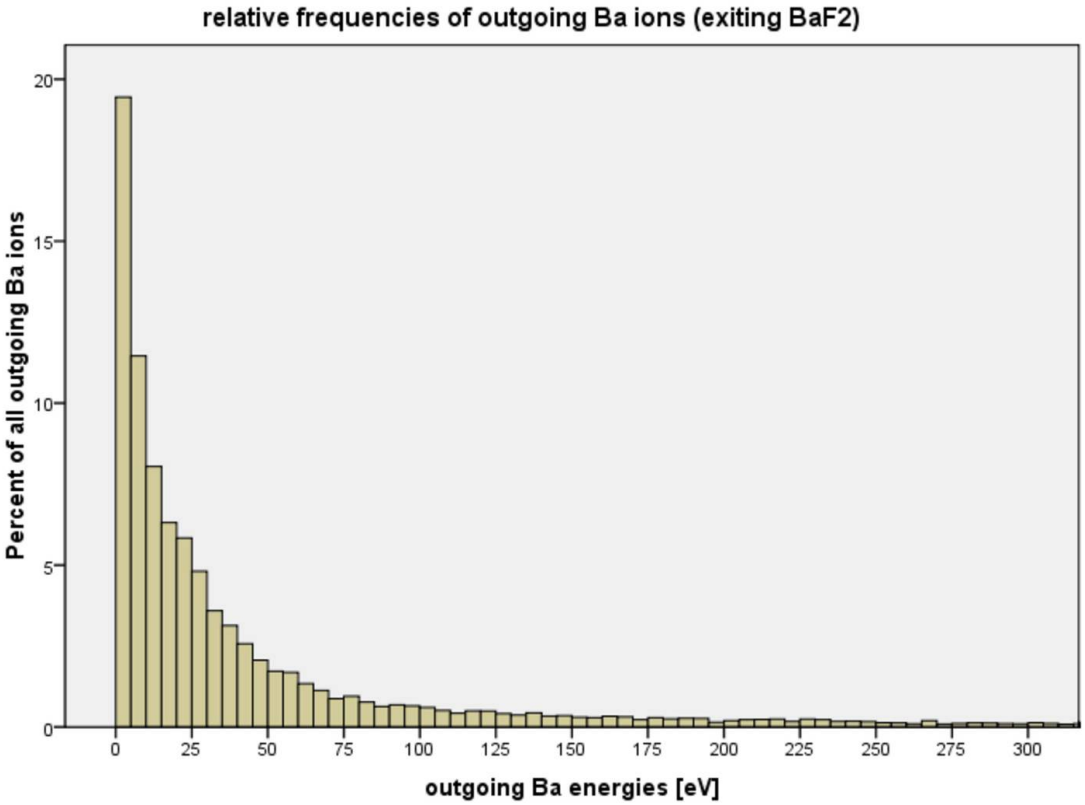

Figure 3.2. Relative frequency histogram for Ba ions leaving the 500 Å BaF_2 layer. The spectrum shows a strong low energy peak with a very long tail into the very high (1 keV) energies. Obtained from a TRIM simulation with 30,000 incident Sm ions on the BaF_2, assigned to different incident angles according to the availability of solid angle.

normal is greatly reduced. At the same time there are few incoming Sm ions at angles close to normal to the BaF_2 due to the limited availability of solid angle coming from the isotropic decay reaction, thus the number of Ba ions that are leaving the BaF_2 layer at those low angles from the normal is greatly reduced as

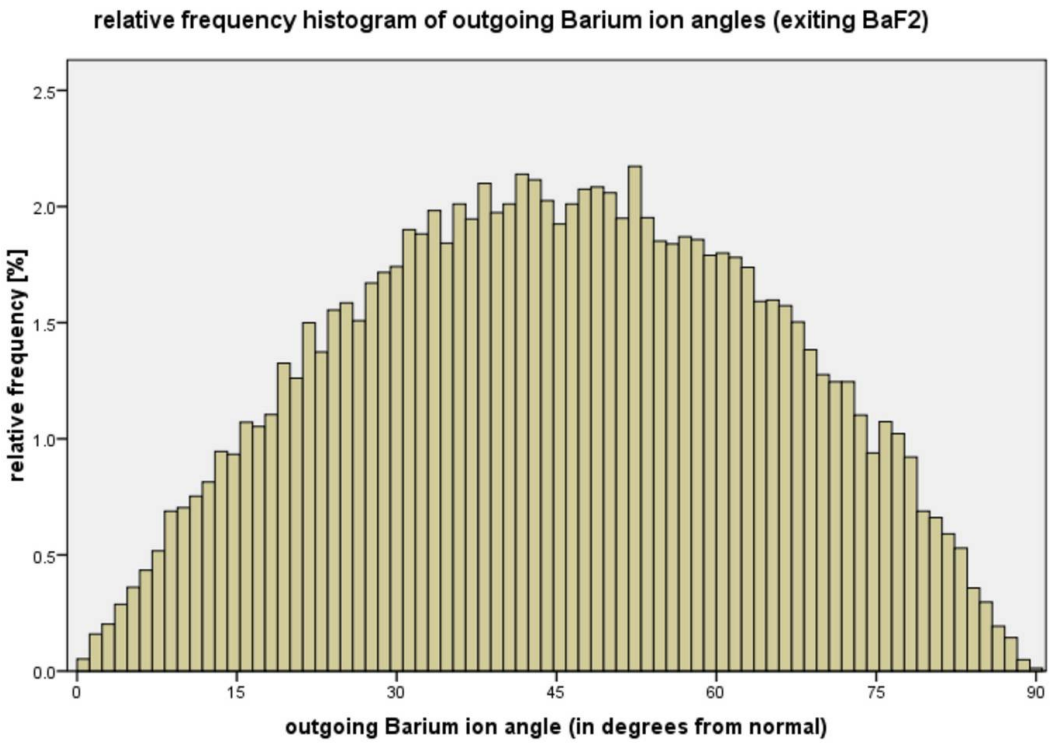

Figure 3.3. Relative frequency histogram for the angles of Ba ions leaving the 500 Å BaF_2 layer, where the angles are measured from the normal. The best fit is sinusoidal with the peak at 45°. The histogram was obtained from a TRIM simulation with 30,000 incident Sm ions on the BaF_2 assigned to different incident angles according to the availability of solid angle.

well. The result is the sinusoidal peak with a maximum at 45° which can be seen in Figure 3.3.

Figure 3.4 and 3.5 show the energy distributions for a given 10° interval of outgoing Ba ion direction. There seems to be only a moderate correlation between energy distribution and outgoing angle for the Barium ions. For lower thicknesses

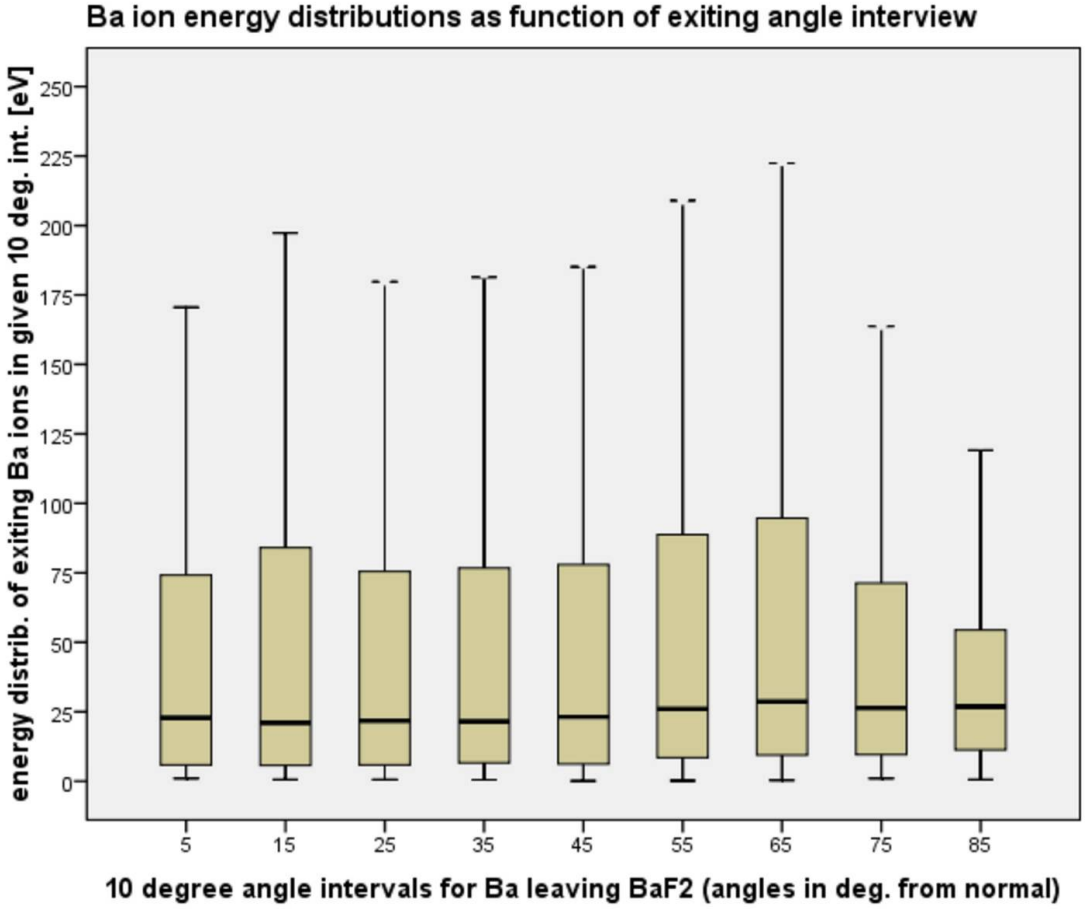

Figure 3.4. Boxplot summaries of the energy distributions (in eV) for exiting Ba ions for different 10 degree solid angle intervals of exit angles obtained from a 30,000 incident Sm ion dataset. The lower limit of box indicates the 25th percentile, the line the median, the upper limit the 75th percentile and the whiskers 1.5 interquartile ranges. In the simulation the number of ions per incident angle was corrected for by solid angle availability such that the outgoing Ba energy distribution approximates an simulated experimental dataset.

of the BaF_2 layer it was found that this correlation was much more pronounced, with higher mean energies for Barium ions leaving at angles closer to the normal.

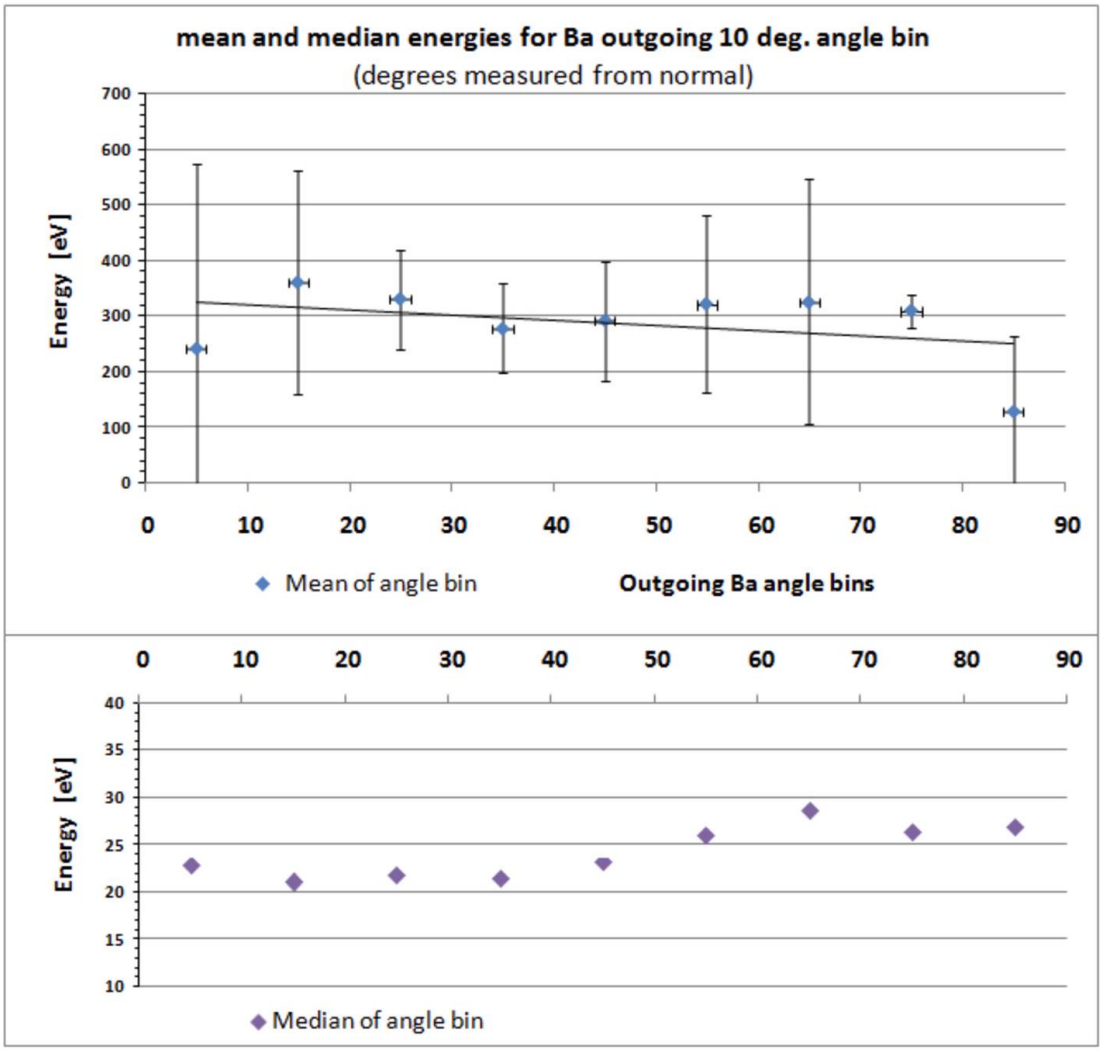

Figure 3.5. (a) Mean energy of exiting Barium ions per 10 degree bins which are centered on the data-points. Degrees are measured from the normal. Mean energy stays roughly the same over the angular range. (b) shows the median energy of exiting Barium ions per 10 degree bins which are centered on the data-points. As the angle moves away from the normal the median energy seems to slightly increase.

This would be expected as the reduced thickness allows a large fraction of the Samarium kinetic energy to be transferred to recoiling and exiting Barium ions which would leave the source closer to the normal direction. However, for the larger BaF_2 target thickness considered in Figures 3.4 and 3.5 this correlation is much reduced due to the averaging nature of a larger number of random ion collisions and energy exchanges. Nevertheless, in the interest of simulation accuracy any remaining correlation between angle and energy distributions was incorporated into the SIMION simulation by using the SRIM Ba ion-by-ion output information as the ion input description for SIMION.

CHAPTER 4

RFQ Theory

4.1. RFQ Setup and Operation

The linear RFQ ion trap has become a popular tool for the manipulation of low-energy ion beams and is used by many groups around the world. An RFQ trap uses a DC well to capture ions in the longitudinal direction (z) and a suitable RF field to constrain the ions radially (x, y) as will be outlined below.

The RFQ shown in Figure 4.1 is available for the Barium source characterization experiment. Four electrode rods with circular cross-sections are mounted in proximity to one another. The rods are separated along the z-axis into segments as can be seen in Figure 4.2. As can also be seen in Figure 4.2 the DC potential is varied across these segments to create a potential well along the longitudinal axis towards the end of the trap. Ions which are trapped in the well can be ejected by lowering the voltage of the last few segments to create a continuous voltage gradient along the trap.

A radial cross-section of the particular RFQ at hand is shown in Figure 4.3. Two electrode segments facing one another will be at the same potential while the other two electrodes will have opposite potential as indicated in Figure 4.3. If

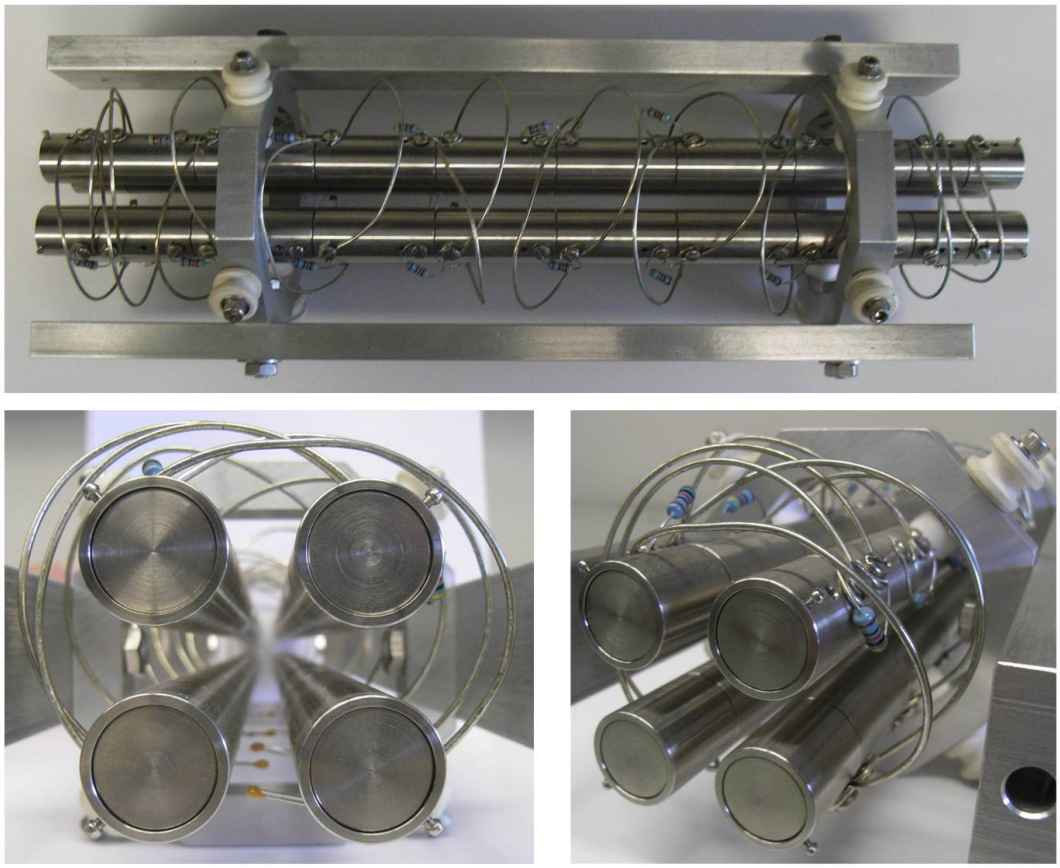

Figure 4.1. Pictures of the RFQ at hand. The total length of the RFQ segments (top) is 34.8 cm. The rods in the bottom view have a radius of 9 mm and are spaced 7.6 mm apart. The minimal distance from the longitudinal RFQ axis to the surface of the rods is 9 mm (r_0).The rods of the RFQ are split into 10 segments. The dimensions of the of the segments can be found in the appendix (9.1).

perturbative contributions to the radial divergence of the field from the axial DC-well potential are neglected, the electric potential in the cross-section associated

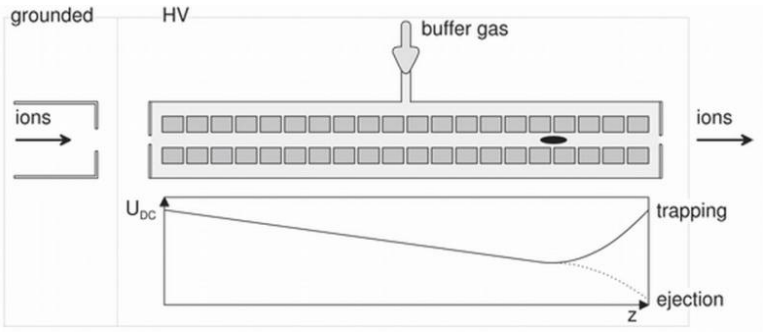

Figure 4.2. Qualitative drawing of a radio-frquency quadrupole ion trap (RFQ). The lower part shows the DC well along the segments of the RFQ in the axial direction. Adopted from [**29**].

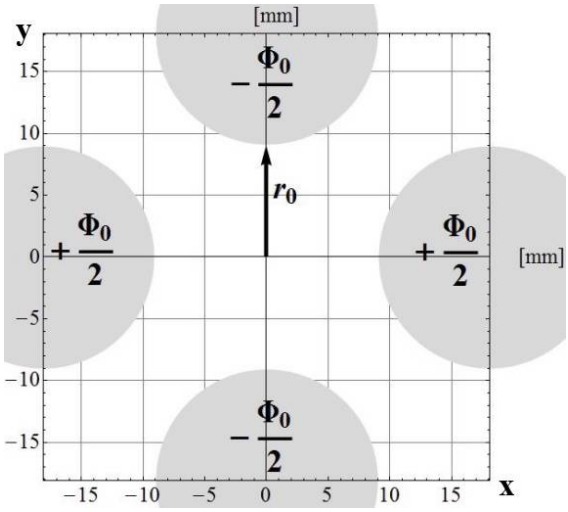

Figure 4.3. Geometric cross-section of the RFQ at hand. Axes are in units of mm. In this and all of the following drawings the horizontal axis is referred to as the x and the vertical as the y-axis.

with the quadrupole field is quadratic in the Cartesian coordinates [**28**]

$$\Phi \sim (ax^2 + by^2) \tag{4.1}$$

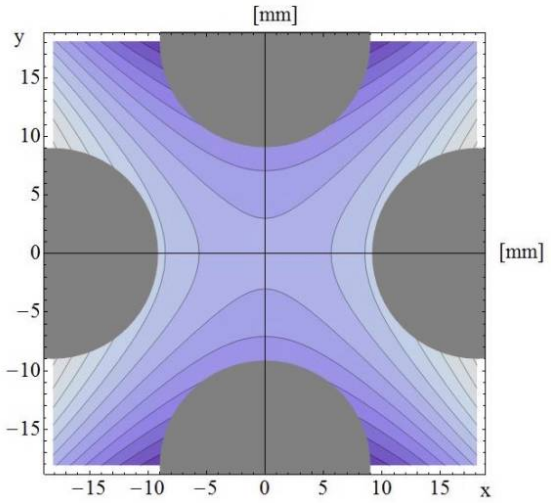

Figure 4.4. Lines of electric equipotential in the cross-section of the RFQ. Color intensity indicates the magnitude of the potential for a given moment in the cycle; darker colors correspond to a lower electric potential. The electric potential gradients are reversed for every half-cycle. The horizontal is designated as the x, the vertical as the y-axis.

which allows for the recovery of the familiar restorative force $F = -\nabla\Phi = -kr$. The RFQ at hand can be treated approximately as having hyperbolically shaped electrodes in the area relevant for the trapping of ions (roughly the area for which $r < r_0$) for which the electric potential is given as

$$\Phi = \frac{\Phi_0}{2r_0^2}(x^2 - y^2) \tag{4.2}$$

which satisfies Laplace's equation:

$$\nabla(\overrightarrow{E}) = -\nabla^2\Phi = -\frac{\Phi_0}{2r_0^2}(2 - 2) = 0 \tag{4.3}$$

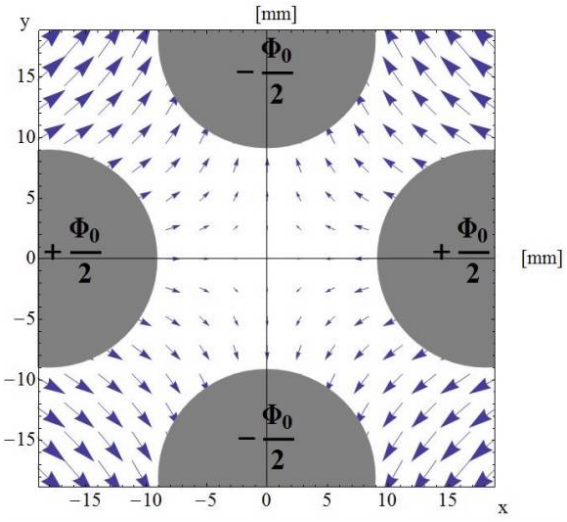

Figure 4.5. Electric field distribution for a moment in the RF cycle. The size of the arrows indicates field strength.

Figure 4.4 depicts the corresponding lines of equipotential. The electric field associated with such a potential follows from $\overrightarrow{E} = -\nabla\Phi$ as

$$\overrightarrow{E} = \frac{\Phi_0}{r_0^2}\begin{pmatrix} -x \\ \\ y \end{pmatrix} \tag{4.4}$$

which is depicted in Figure 4.5 for a positive value of Φ_0. For the quadrupole to act as an ion trap the supplied electric potential should be of the form

$$\Phi_0 = U_{shift} + V_{RF}\cos\omega_{RF}t \tag{4.5}$$

where $V_{RF} = V_{RF-pp}$ is the peak-to-peak amplitude of an RF-potential with angular frequency ω_{RF} and where the potential shift U_{shift} between the electrode pairs introduces an operational parameter which allows for the utilization of the RFQ

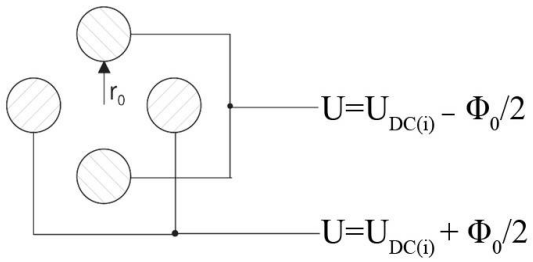

Figure 4.6. The segments belonging to one rod of the RFQ will be at the same + or -$\frac{\Phi_0}{2}$ potential offset along the entire length of the RFQ.

as a mass filter (or more precisely, a filter for mass-to-charge ratios). To clarify, a given pair of electrodes in segment i along the trap will be at the potential

$$U_{total} = U_{DC(i)} \pm \frac{\Phi_0}{2} = U_{DC(i)} \pm \frac{U_{shift} + V_{RF} \cos \omega_{RF} t}{2} \tag{4.6}$$

$U_{DC(i)}$ will vary with every segment i along the RFQ and be the same for the 4 electrodes of that RFQ segment. As Figure 4.6 indicates in the cross-section along the RFQ, all segments along two rods across from one another will experience the same $+\frac{\Phi_0}{2}$ potential shift at a given moment in time, while the other two rods will be $-\frac{\Phi_0}{2}$ shifted. This potential shift is applied in addition to the $U_{DC(i)}$ which varies with every RFQ segment.

The RF voltage provides the trapping of the ions in both Cartesian directions in the transverse plane. The electric force is weakest in the center of the trap as can be seen in Figure 4.5. The positively charged ions experience an attractive force in one direction for a moment in the RF cycle whose magnitude linearly depends on their distance from the center of the trap (e.g. $\overrightarrow{F_x} = -k\,|x|$). This means

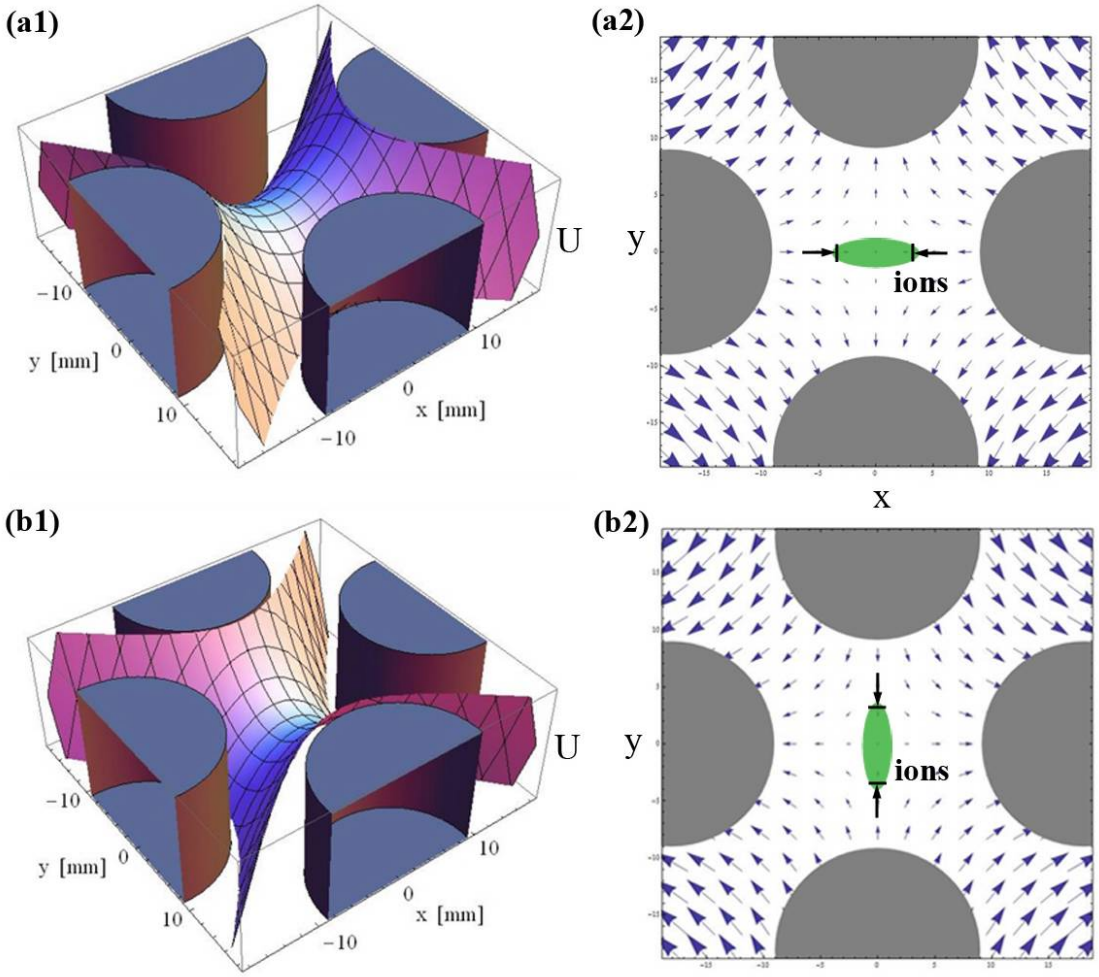

Figure 4.7. The two top drawings (a1) and (a2) describe the same moment in time ((b1) and (b2) respectively). Electric potential (on the left) and electric field distributions (on the right) are shown in cross-section of the RFQ for instants separated by half a RF cycle. The black arrows on the right show the force exerted by the field on the ion bunch in the center of the trap. The further the ions are from the center, the larger is the attractive force by which they are pulled back into the middle. This inhomogeneity in field and thus force strength keeps the ions trapped given a suitable RF frequency.

the farther the ions are in a given Cartesian direction from the center of the trap the stronger is the focusing force they experience which compresses them in that direction. The ions are defocused in the other orthogonal direction but given a suitable RF on average less so due to their compressed spatial configuration in the "defocusing" direction. Herein lies the key to trapping the ions; due to their 180° phase lag with the field, the compressing force they experience is the strongest in the direction in which they are most extended at that moment in the cycle (Figure 4.7, right). Half a RF cycle later the field "flips" in the other direction (Figure 4.7, top vs. bottom) and focuses the ions in that direction in which they are now most extended. As a result, overall in time the ions experience a stronger focusing force than they do a defocusing force in both directions, and are thus trapped radially.

4.2. The Mathieu Equation and Parameters

In the transverse plane the equations of motion of the ion with charge e and mass m are given via $\overrightarrow{F} = e\overrightarrow{E}$ as

$$\begin{pmatrix} \ddot{x} \\ \\ \ddot{y} \end{pmatrix} = \frac{e}{mr_0^2}(U_{shift} + V_{RF}\cos\omega_{RF}t) \begin{pmatrix} -x \\ \\ y \end{pmatrix} \tag{4.7}$$

If the following non-dimensional substitution is made for the time variable [**28**]

$$\tau = \frac{\omega_{RF}t}{2} \tag{4.8}$$

and we take u to represent either of the spatial variables x and y, the acceleration terms in the equation of motion can be rewritten as

$$\frac{d^2u}{dt^2} = \frac{d}{dt}(\frac{du}{dt}) = \left(\frac{d\tau}{dt}\right)^2 \frac{d}{d\tau}(\frac{du}{d\tau}) = \frac{\omega_{RF}^2}{4}\frac{d^2u}{d\tau^2} \tag{4.9}$$

and consequently the equation of motion as

$$\frac{d^2}{d\tau^2}\begin{pmatrix} x \\ y \end{pmatrix} + \frac{4e}{mr_0^2\omega_{RF}^2}(U_{shift} + V_{RF}\cos 2\tau)\begin{pmatrix} x \\ -y \end{pmatrix} = 0 \tag{4.10}$$

If the following further non-dimensional substitutions are introduced

$$a_x = \frac{4eU_{shift}}{mr_0^2\omega_{RF}^2} = -a_y \qquad q_x = \frac{2eV_{RF}}{mr_0^2\omega_{RF}^2} = -q_y \tag{4.11}$$

the Mathieu equation is recovered:

$$\frac{d^2u}{d\tau^2} + (a_x + 2q_x\cos 2\tau)u = 0 \quad . \tag{4.12}$$

4.3. Stability

The solutions to the Mathieu equation have been the subject of much technical literature [**25, 26**]. For our purposes it suffices to indicate that the general solution to the Mathieu equation is a series expansion of exponentials which only yields stable solutions if the exponential coefficients are purely imaginary and certain numerical conditions on the Mathieu parameters 'a' and 'q' are fulfilled, which are indicated in Figure 4.8. The Mathieu parameter 'a' depends on the DC voltage

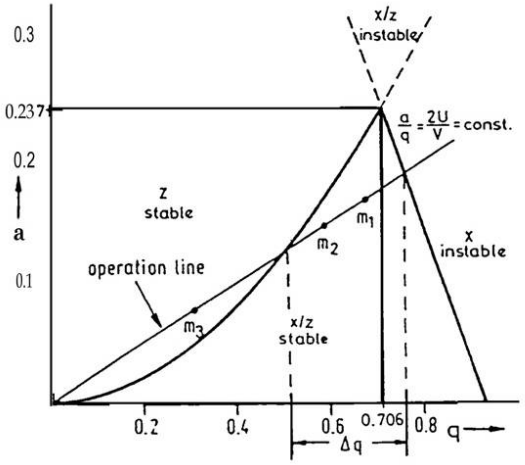

Figure 4.8. Stability regime for the ions in the RFQ in a-q space, where a and q are the Mathieu parameters. The bounded roughly triangular region is the region of simultaneous stability in both transverse directions (x and y, here referred to as z). Taken from [**28**].

differential between the two electrode pairs within one segment (U_{Shift} as part of $\frac{\Phi_0}{2}$) and introduces mass selectivity by defining the "operation line" and accessible domains of stability for different charge-to-mass ratios given U_{Shift} as an experimental parameter. In Figure 4.8 it can be seen that for a given V through U_{Shift} the slope of the operation line can be varied and thereby a given mass can be made to be unstable in the ion trap (point "m_3" in Figure 4.8). This allows the trap to be fine-tuned as a mass filter. We however will not make such use of the trap and thus will not introduce a non-zero U_{Shift}; our Mathieu parameter 'a' thus simplifies to a = 0. The weaker criterion of ion stability in the trap then becomes [**29**]

$$q = \frac{2eV_{RF}}{mr_0^2\omega_{RF}^2} < 0.908 \tag{4.13}$$

It can further be shown following the formalism of the series expansion [**25**] that the stable orbits can be described as a superposition of harmonic micro- and macro-motions [**30**] (due to the stability criterion of purely imaginary exponent coefficients in the series expansion) which are associated with the different n-th order terms in the series expansion. In particular it can be shown that the frequencies in stability are limited to integer-order values for n

$$\omega_n = (2n + \beta)\frac{\omega_{RF}}{2} \tag{4.14}$$

where the parameter β reduces to $\beta = \frac{q}{\sqrt{2}}$ in our Mathieu parameter $a = 0$ simplification. Thus the frequencies in stability can be given as

$$\omega_n = (n + \frac{q}{2\sqrt{2}})\omega_{RF} \tag{4.15}$$

where the lowest order $n = 0$ term is associated with the macro-motion of the particle, and the higher order terms with the micro-motion. So to leading order the oscillation frequency of the ion in the trap is given by $\omega_{ion} = \frac{q}{2\sqrt{2}}\omega_{RF}$. In analogy with the simple harmonic oscillator [**27**] we can define a restorative spring constant k of the ions in the radial pseudo-potential well

$$\sqrt{\frac{k}{m}} = \omega_{ion} = \frac{\omega_{RF}}{2\sqrt{2}}\frac{2eV_{RF}}{mr_0^2\omega_{RF}^2} \tag{4.16}$$

which reduces to

$$k = \frac{1}{2m}(\frac{eV_{RF}}{r_0^2\omega_{RF}})^2 \tag{4.17}$$

We can use our knowledge of the harmonic oscillator by employing $F_r = -e\nabla V_{PS}(r) = -kr$ in

$$\int_0^r \nabla V_{PS}(r')dr' = \int_0^r \frac{r'}{2m}\frac{eV^2}{r_0^4\omega_{RF}^2}dr' \tag{4.18}$$

and thus determine $\mathrm{V}_{PS}(\mathrm{r})$ as

$$V_{PS}(r) = \frac{r^2}{4m}\frac{eV^2}{r_0^4\omega_{RF}^2} \tag{4.19}$$

which implies a potential depth $V_{PS}(r = r_0)$ of

$$V_{PS} = \frac{eV_{RF}^2}{4mr_0^2\omega_{RF}^2} = \frac{qV_{RF}}{8} \tag{4.20}$$

4.4. The full Pseudo-Potential

Following [**29**] and Figure 4.2 on page 27, the confinement along the axis is provided by a DC potential well with its minimum towards the "end" of the RFQ. As usual, to leading order the shape of the potential minimum can be approximated as a parabola in the axial direction

$$V(r = 0, z) = \frac{U_{DC}}{z_0^2}z^2 \tag{4.21}$$

where z_0 is a characteristic length of the trap (of the order of $\frac{1}{2}$ of the RFQ length) and $D_z = U_{DC}$ is the DC potential well depth over that length. $\frac{U_{DC}}{z_0^2}$ would thus be a measure of the steepness of the potential. In our derivation of the radial confinement we have so far neglected the radial confinement in this potential well. However, Laplace's equation

$$\nabla^2 V(r,z) = 0 \tag{4.22}$$

demands that the radial field diverges at its longitudinal focal point $z = z_0$ [**29**], thereby counteracting part of the radial pseudo-potential $V_{PS} = \frac{qV}{8}$ derived above. In cylindrical coordinates this requirement is specified via the Laplacian as

$$\frac{1}{r}\frac{\partial}{\partial r}(r\frac{\partial V}{\partial r}) = \frac{1}{r}\frac{\partial V}{\partial r} + \frac{\partial^2 V}{\partial r^2} = -\frac{\partial V}{\partial z^2} = -2\frac{U_{DC}}{z_0^2} \tag{4.23}$$

which similarly to Equation 4.3 is satisfied by

$$V(r,z) = \frac{U_{DC}}{z_0^2}(z^2 - \frac{r^2}{2}) \tag{4.24}$$

The effective potential depth of the pseudo potential $\overrightarrow{V}_{PS}(r = r_0, z = z_0)$ in both directions is thus given by

$$V_{PS}(r_0) = \frac{qV_{RF}}{8} - \frac{U_{DC} r_0^2}{2z_0^2} \tag{4.25}$$

$$V_{PS}(z_0) = U_{DC} \tag{4.26}$$

This effectively limits the maximum longitudinal confinement that can be applied through U_{DC}. However, in the later discussed regime of operational parameters for the RFQ at hand, the $-\frac{U_{DC}r_0^2}{2z_0^2}$ terms has the character of a perturbation. For example, for the "suggested RFQ configuration" to be introduced later the $\frac{U_{DC}r_0^2}{2z_0^2}$ term contributes a 0.2 V reduction to $V_{PS}(r_0) = 22.5\ V$.

CHAPTER 5

SIMION RFQ Simulations

5.1. Introduction to SIMION

SIMION was developed in the late 70's and was implemented for personal computers in the 80's by D. Dahl at the Idaho National Engineering and Environmental Laboratory (INL). It is widely used in ion optics simulations to solve for electrostatic field potentials numerically and to calculate the resulting ion trajectories at arbitrarily high precision using a standard fourth order Runge-Kutta method [**32**]. Figure 5.1 (a) depicts a model of the RFQ with the measurements discussed above highlighting the separate electrode pairs in different colors created in version 8.0 of the program [**33**]. Figure 5.1 (b) shows trajectories with the RFQ operating at a stable q; in (c) a potential energy surface in a cross-section of the RFQ can be seen as represented by the program (c.f. Figure 4.7, left).

5.2. SRIM data import into SIMION

To simulate the trajectory of Ba ions in the RFQ, it was first necessary to represent the energy and angular distribution of the Ba ions as they leave the BaF_2 source to SIMION. It was attempted to describe the distributions analytically and

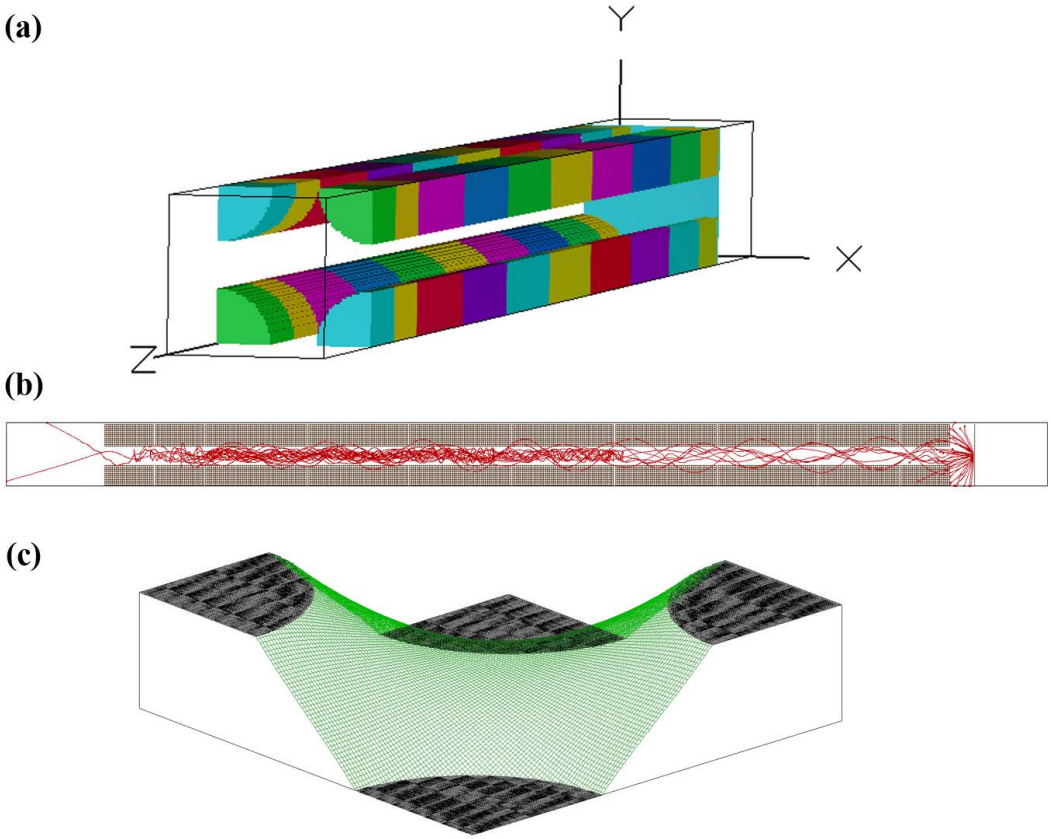

Figure 5.1. (a) A reproduction of the RFQ at hand in SIMION. The side of the RFQ that faces the source is shown in the back; the depicted plate is used in some of the simulations discussed below to change the potential at which the source is held. Different electrode segments are shown in different colors. (b) shows a XZ perspective on the RFQ with ion trajectories starting on the right at a plate 10 mm in front of the RFQ as shown in (a). Two ion trajectories can be seen to escape the RFQ to the left in the positive z direction. (c) shows the potential surface view available in SIMION to depict the electrostatic potential; shown here are two electrode pairs in a cross-section in the RFQ at opposite (Φ-shifted) potentials (c.f. Figure 4.7 on page 31, left).

then to recreate them by inverting the probability density functions in a Monte-Carlo approach; however the details of the correlation between angular and energy distribution (c.f. Figure 3.4) complicated this approach tremendously.

Instead, the outgoing Ba ion specifications were fed to SIMION ion by ion by converting the output format of SRIM into an input format of SIMION (.ion). Particular attention had to be paid to a suitable mapping and adjustment of the coordinate and angular distributions; SRIM implictly chooses a specific plane normal to the BaF_2 layer in its simulation of the penetration of BaF_2 by the Samarium ions, a fact which results in a preferential angular direction of Ba release as depicted in Figure 5.2 (a). Figure 5.2 (b) shows the ion trajectories corrected for the isotropic nature of the source while maintaining the ion trajectories' angle with the normal and its associated energy correlation (c.f. Figure 3.4).

5.3. Simulations of the RF Fields and Gas Collisions

To simulate the RF fields according to the theory outlined above, as well as the ions' interaction with the buffer gas (Helium) at a definable pressure and temperature, SIMION can execute programming code during the flight of the ions and update the potentials accordingly at every time-step (which can freely be chosen to arbitrary accuracy). Guy Savard has originally written programming code in SIMION's PRG language to model the interactions in the RFQ using a Monte-Carlo implementation of the interatomic and field interactions. Matthew Sternberg has consequently refined the code and provided it for this analysis. The

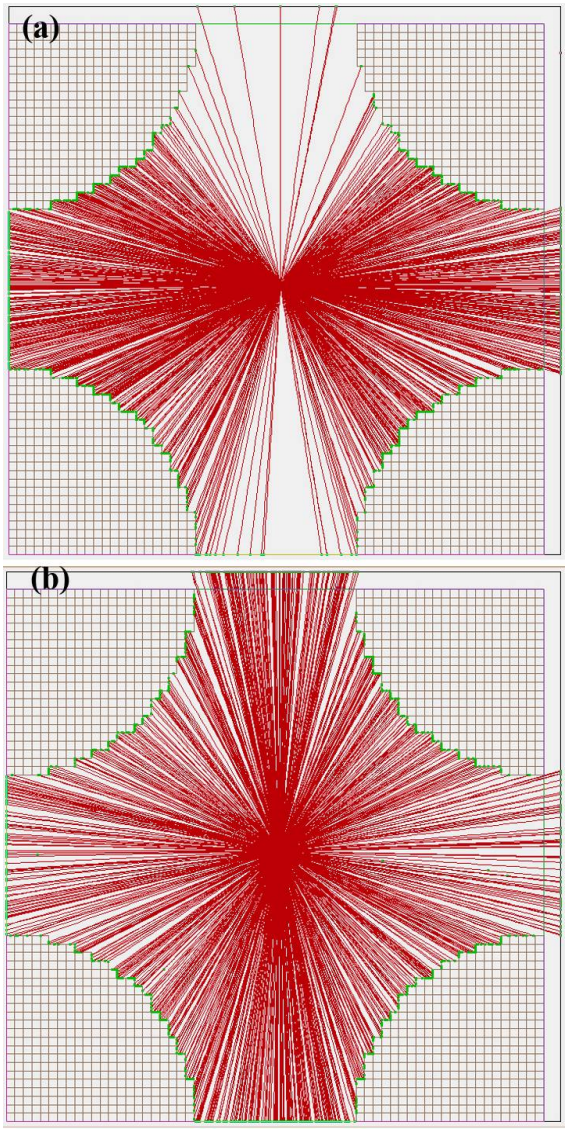

Figure 5.2. XY-view of the Ba ions exiting the source seen from inside the RFQ. (a) depicts the ion trajectories as they are given by SRIM upon a direct mapping of the coordinate systems; (b) shows the ion trajectories corrected for the isotropic character of the Ba source.

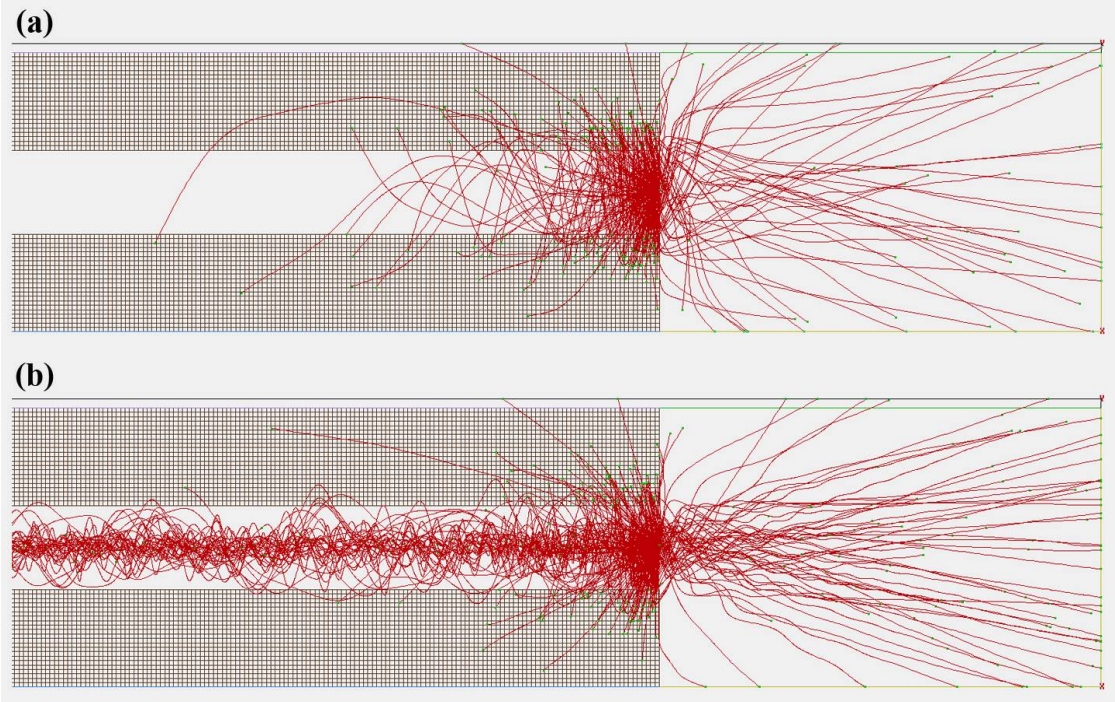

Figure 5.3. XZ-side view of Ba ion trajectories originating at the center of the entrance of the RFQ in the right half of the picture. (a) the RFQ operated with a choice of V_{RF} and ω_{RF} which results in a value for the Mathieu parameter q which indicates instability for Ba ions; (b) the same RFQ operated with q in the range of stability. Ions are being trapped and guided to the minimum of the axial U_{DC}-potential (to the left of the section shown).

code was then adjusted for the particular RFQ geometry at hand and extended with data recording options for different definable ion time-of-flight (TOF) criteria (c.f. Section 7.4 on page 64).

Savard and Sternberg follow Mason et al. [**31**] who suggest the formulation of the potential between an ion and a molecule as

$$\varphi = \frac{\epsilon}{2}[(1+\gamma)(\frac{r_m}{r})^{12} - 4\gamma(\frac{r_m}{r})^6 - 3(1-\gamma)(\frac{r_m}{r})^4] \tag{5.1}$$

where r is the separation between the ion and the molecule, "ϵ is the depth of the potential energy minimum, r_m is the value of r for which $\varphi(r)$ is a minimum, and γ is a third parameter which may be considered a measure of the relative strength of the dispersion plus the charge-induced quadrupole energy." The $(\frac{r_m}{r})^{12}$ term represents a hard core repulsive interaction, the $(\frac{r_m}{r})^6$ term accounts for the induction of a quadrupole moment by the Ba ion in the Helium atom while $(\frac{r_m}{r})^4$ represents the longer range induced dipole interaction. The parameters of this potential are determined to reproduce the experimental ion mobility data [**31**]. From $\varphi(r)$ the scattering angle χ can be calculated as a function of impact parameter b and energy E and stored in a table which the Monte-Carlo simulation accesses to calculate the collisions, and hence the energy loss of the ions in the gas.

Figure 5.3 depicts ion trajectories generated by the simulation code for an unstable (a) and a stable (b) value for the q parameter which is defined as (Equation 4.11)

$$q = \frac{2eV_{RF}}{mr_0^2\omega_{RF}^2} \tag{5.2}$$

with a pseudo-potential given as (Equation 4.25)

$$V_{PS}(r) = \frac{qV_{RF}}{8} - \frac{U_{DC}}{2z_0^2} r^2 \tag{5.3}$$

$$V(z) = \frac{U_{DC}}{z_0^2} z^2 \tag{5.4}$$

These are reproduced here for reference allowing for an approximate measure of stability, the simulation code itself makes no use of the approximating pseudo-potential.

CHAPTER 6

SIMION Results: Variation of operational Parameters to maximize Capture Efficiency (CE)

As derived above, q is taken to be a direct measure of the stability of the ions in the RFQ; V_{RF} and U_{DC} directly determine the depth of the (pseudo-)potential in the trap. External parameters such as the gas pressure and geometric location of the source with respect to the RFQ as well as the DC-potential in front of the trap further influence the capture efficiency on the RFQ (understood as ions trapped in the RFQ as a fraction of ions leaving the BaF_2 source).

These parameters were varied with respect to one another to attempt to find optimal operation parameters; their effects on RFQ capture efficiency as simulated by SIMION are presented below.

In the following, until the parameters are varied explicitly, the default potential well depth is set to $U_{DC} = 20\ V$. The potential well is slightly asymmetric with the potential being 2.5 V higher at the exit of the RFQ than at the entrance (as shown in Figure 7.5 (b)). It was found that this potential shape minimizes the fraction of ions which escapes the RFQ axially for a given potential depth U_{DC}, or at least shows higher capture efficiencies than a symmetric potential well of the same depth. The BaF_2 source is considered to be a point source in the center of the

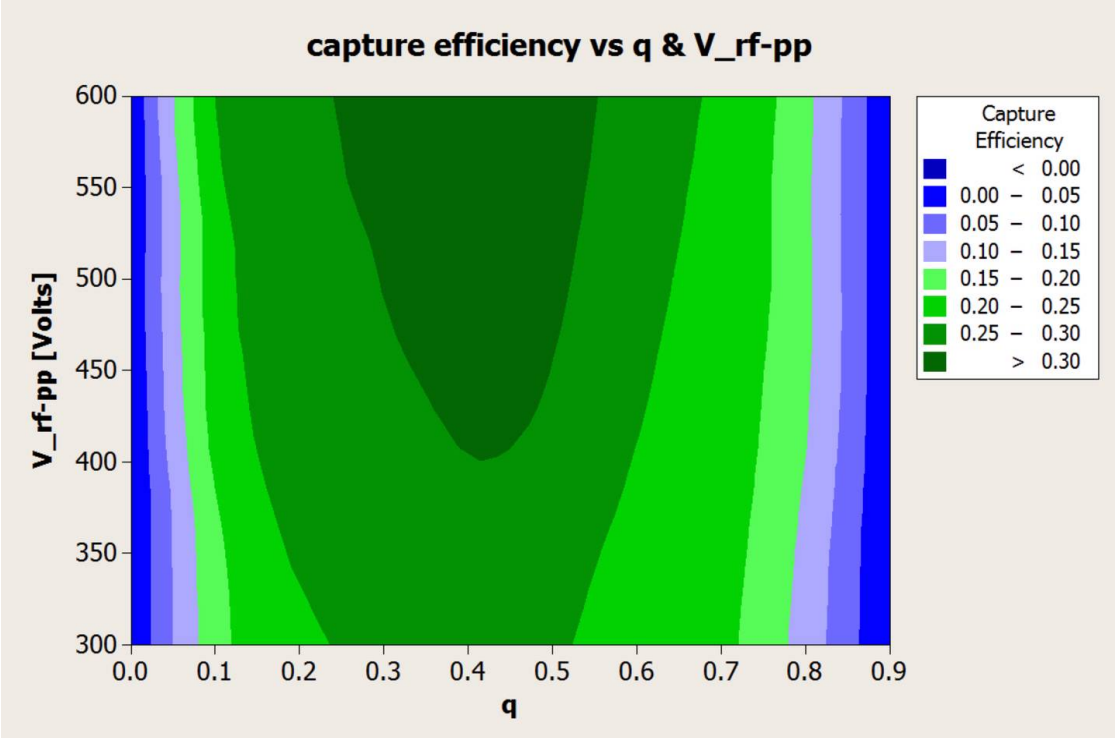

Figure 6.1. Contour plot indicating different capture efficiencies (ions captured as fraction of ions leaving the source) as a function of both different V_{RF} and Mathieu parameter q (which for a given V_{RF} is varied via ω_{RF}). Darker shades of green indicate higher capture efficiencies. The data indicate that for a given q a higher value for V_{RF} will increase capture efficiency. The peak capture efficiency for a given V_{RF} seems to be obtained for values of q between 0.3 and 0.5. The data-points are the result of a full SIMION simulation of gas collisions in the RFQ with 887 Ba ions leaving the source per data-point; the above chart incorporates 27 data-points. The errors associated with a representative sample of data-points are shown in Figure 6.3.

entrance of the RFQ. Throughout the entire following analysis the gas temperature is set to 300 K and Ba ions are considered to carry a single positive charge.

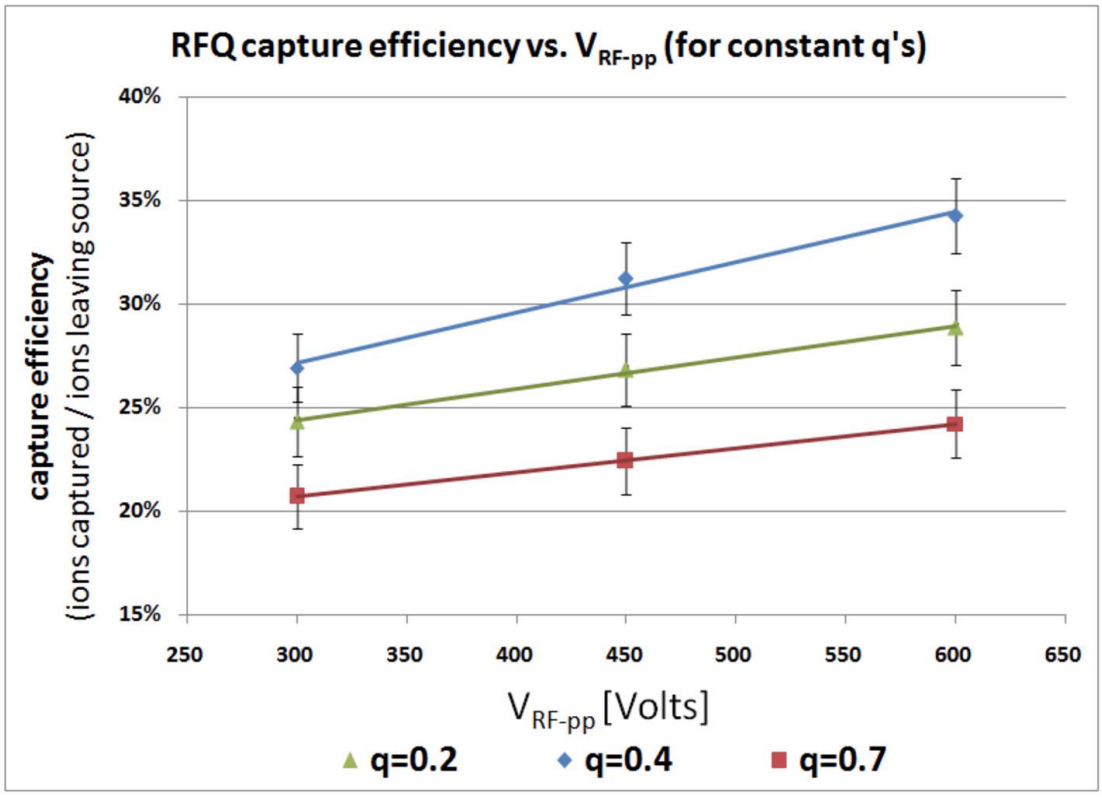

Figure 6.2. RFQ capture efficiency (ions captured as fraction of ions leaving the source) for different values of q (bottom, red: q = 0.7; middle, green: q = 0.2; top, blue: q = 0.4). For a given value of q the RF voltage V_{RF} and frequency ω_{RF} are varied. The data suggests that for a given value of q a higher V_{RF} will yield higher capture efficiencies as suggested by the equation of the radial pseudo-potential $V_{PS}(r)$ (equation **??**). The data-points were obtained with a full SIMION simulation of gas collisions in the RFQ with 887 Ba ions leaving the source per data-point.

6.1. CE: Variation in q and V_{RF}

Equation **??** suggests that at a constant q corresponding to a stable solution an increase in V_{RF} will monotonically deepen the potential well and should thus

increase capture efficiency. In Figure 6.1 both V_{RF} and q were varied and this relationship was indeed observed; for a given q a maximization of V_{RF} was found to increase capture efficiency in all cases. Figure 6.2 shows the same again for three choices of q (q=0.2, 0.4, 0.7) with the associated error bars; the monotonic increase of capture efficiency with potential well depth via V_{RF} seems to be clearly indicated by the positive slope of the linear regression fits.

6.2. CE: Variation of q with constant V_{RF}

Having determined that a maximization of V_{RF} will maximize capture efficiency, in the following analysis V_{RF-pp} is set to 450 V which is close to the maximum V_{RF-pp} feasible within the typical experimental constraints. In Figure 6.3 V_{RF-pp} is fixed to this maximum value and ω_{RF} is varied to determine the capture efficiency for different values of the stability parameter q. Given V_{RF} the optimal q seems to be $q \approx 0.4$. Thus in the following discussion for the variation of the other parameters the operating parameters will be held constant at $V_{RF-pp} = 450\ V$ and $q = 0.4$ which implies an angular frequency of $\omega_{RF} = 708.6\ kHz$.

The loss of ions escaping along the axis of the RFQ (as can be seen in Figure 6.7 (b) for example) already seems to be minimized through the aforementioned slightly asymmetric shape of the U_{DC} potential well (the red data series in Figure 6.3). In simulations in which the U_{DC} potential well was symmetric between entrance and exit of the RFQ the loss of ions from the RFQ through axial escape was

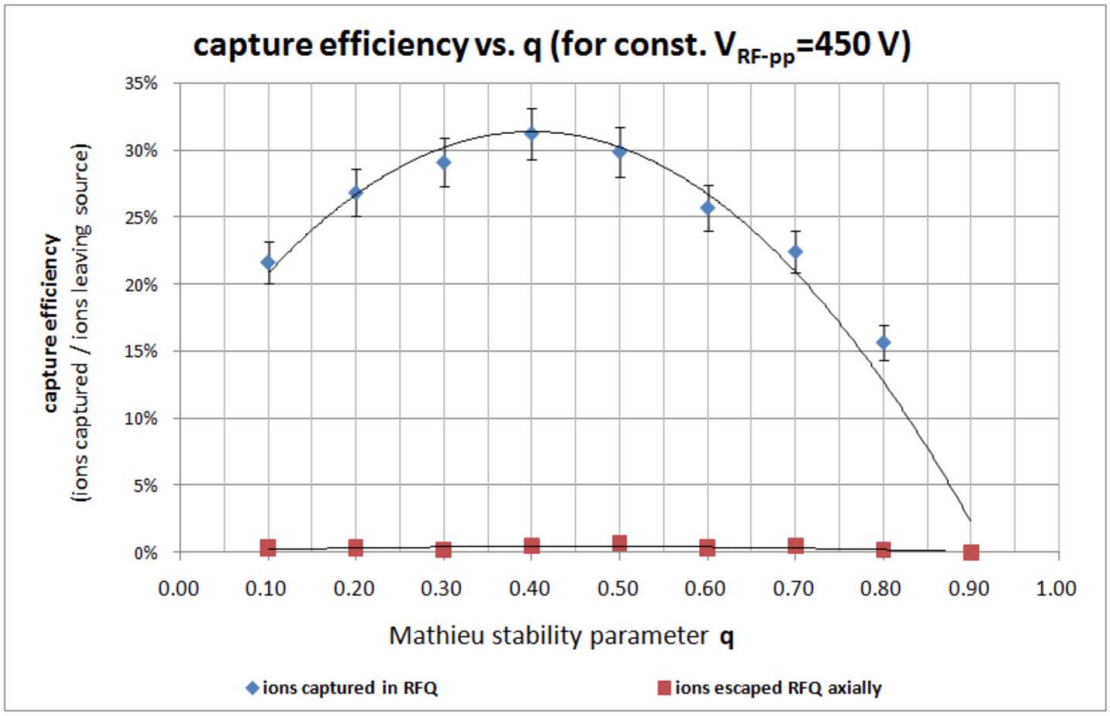

Figure 6.3. For a given maximal $V_{RF-pp} = 450\ V$ the capture efficiency (ions captured as fraction of ions leaving the source) is given as a function of q where q is varied via ω_{RF}. The fit is a second order polynomial to guide the eye. The data suggests a peak in capture efficiency for a q of 0.3 to 0.5. The data-points were obtained with a full SIMION simulation of gas collisions in the RFQ with 887 Ba ions leaving the source per data-point.

as high as 5% for a potential well depth of $U_{DC} = 20V$, even given other "optimal" operation parameters (compared to a loss of <1% in axial direction in Figure 6.3).

6.3. CE: Gas Pressure

Increasing the gas pressure within the RFQ has a similar effect to increasing V_{RF} in that it seems to monotonically increase capture efficiency - that is the

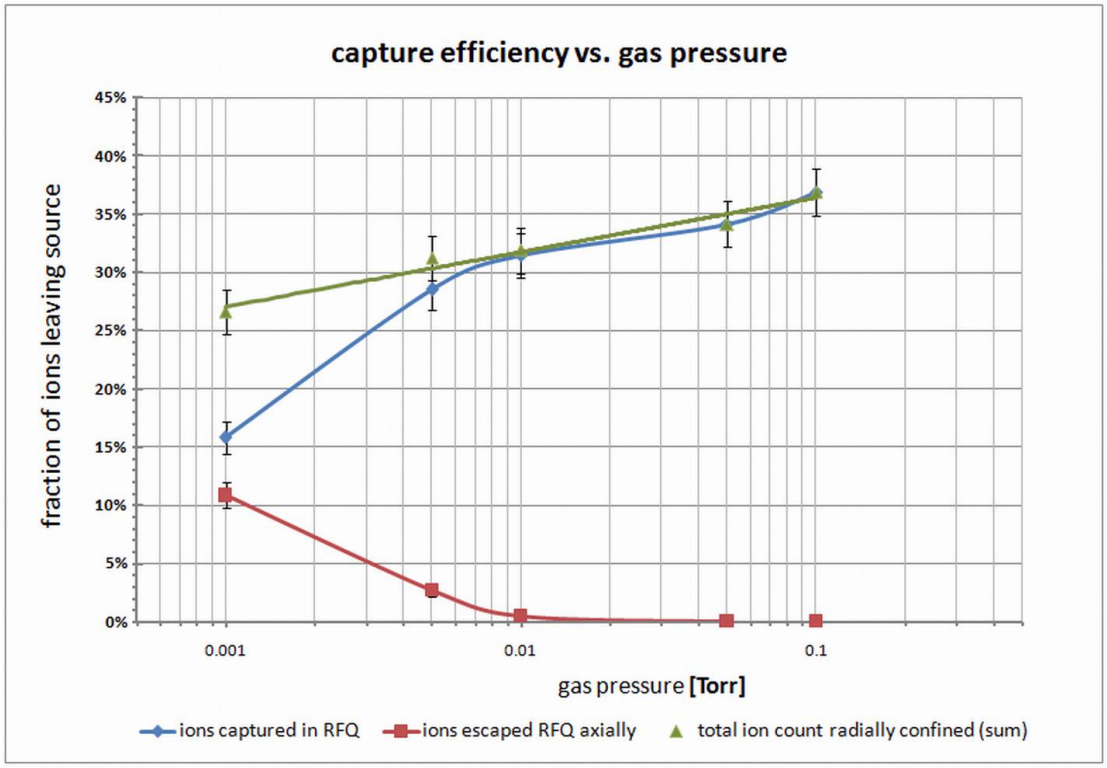

Figure 6.4. Capture efficiency of the RFQ (ions captured as fraction if ions leaving the source) for different gas pressures while holding V_{RF} and ω_{RF} constant such that $V_{RF-pp} = 450\ V$ and $q = 0.4$ (implying that $\omega_{RF} = 708.6\ kHz$). As the gas pressure is increased capture efficiency increases monotonically while the number of ions that leave the RFQ on the side opposite to the source monotonically decreases. The sum of both captured and escaping ions seems to increase moderately as well with an increase in gas pressure. The data-points were obtained with a full SIMION simulation of gas collisions in the RFQ with 887 ions leaving the source per data-point.

fraction of ions which are both radially as well as axially confined in the RFQ (Figure 6.4). Previous runs with symmetric potential wells suggested that the increase in capture efficiency with increasing gas pressure stems from an increase

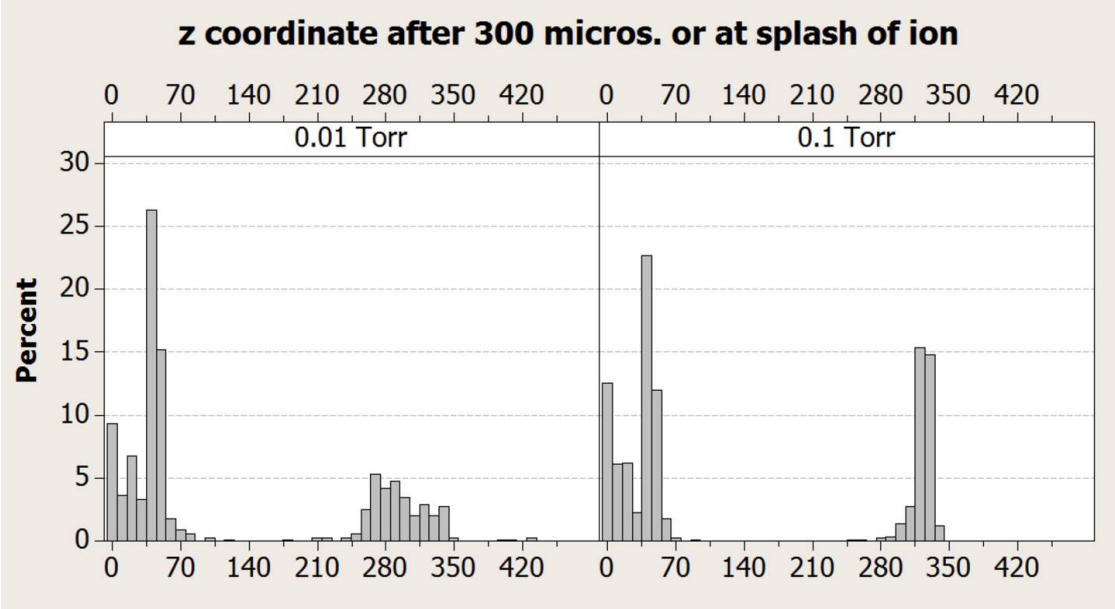

Figure 6.5. Position of ions in mm after 300 μs or at splash (collision) of ion as function of different gas pressures. Both data-series represent 887 Ba ions leaving the BaF_2 source. The RFQ is positioned in the entrance of the source at z=40 mm.

in axial confinement. Beyond 0.01 Torr however the sum of the number of ions captured in the RFQ continues to increase moderately (Figure 6.4, blue and green data-points) while the number of ions which escape the RFQ axially in the forward direction (to the left in all RFQ pictures) does not diminish further (red data-points) and thus cannot be the source of the increase in captured ions. This suggests that either the increase in gas pressure increases radial confinement and keeps ions from colliding with the electrodes early on in their trajectories (which they would at lower pressures) or that due to the slighty asymmetric shape the increased gas pressure manages to confine ions which have initially "bounced off"

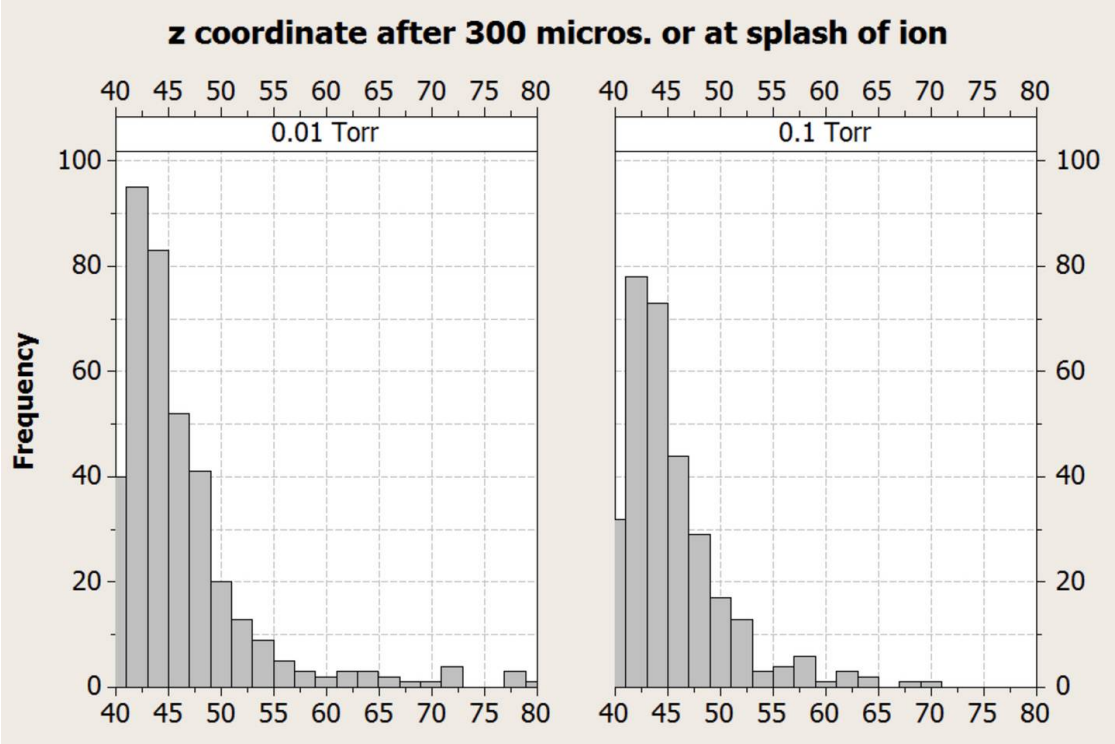

Figure 6.6. "Terminal position" of the Ba ions on collision with the electrodes or after 300 μs. The depicted cases are very likely to be collision events, as no ion can be axially localized by the electric potentials in the entrance of the RFQ for 300 μs. All other RFQ parameters in the two configurations are the same except for the gas pressure. Frequency count is out of 887 ions which left the BaF_2 layer originally.

the potential wall towards the end of the RFQ and would have escaped the RFQ in the backwards direction, passing the source on their way out. An increase in radial confinement would be suprising given the width of the RFQ, it would mean that the change in gas pressure serves to increase radial confinement and keep ions

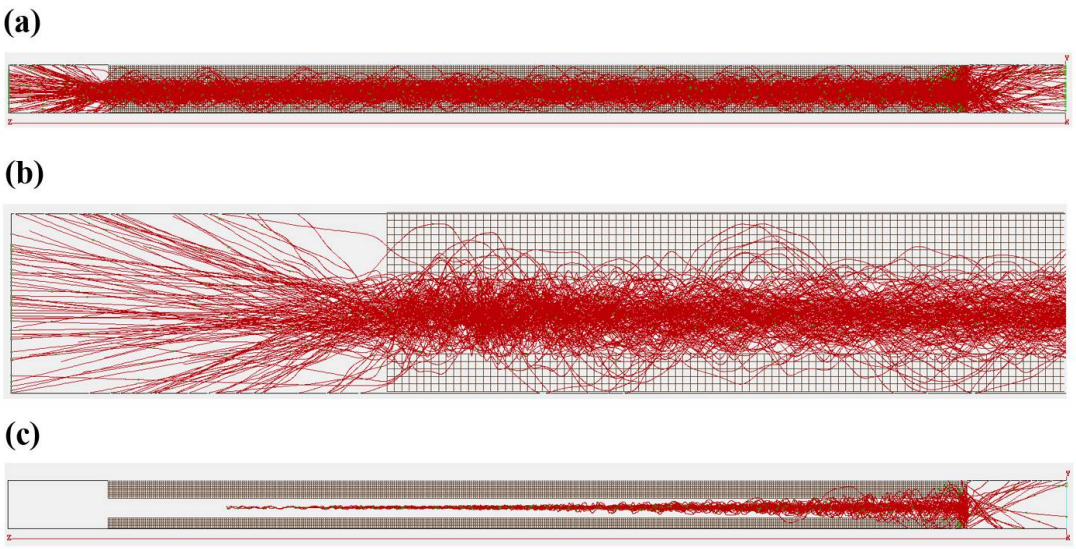

Figure 6.7. Ion trajectories for different gas pressures at $V_{RF-pp} = 450\ V$ and $q = 0.4$. The source is positioned at the entrance of the RFQ on the right (seen in (a) and (c). In (a) & (b) a gas pressure of $P_{Gas} = 0.001\ Torr$ is not sufficient to confine the ions axially, they "spill out" of the RFQ on the left side opposite to the source. (b) provides a close-up of this RFQ "exit" region. (c) In contrast, a gas pressure of $P_{Gas} = 0.05\ Torr$ confines the ions efficiently both radially as well as axially, they cool quickly and are efficiently localized in the minimum of the DC potential well along the axis (c.f. the z-coordinate distribution in Figure 6.5, right).

from crashing into electrodes with the ion having travelled only a distance of the order of 10 mm ($\approx r_0$).

Figure 6.5 shows the ion positions after 300 μs or when they "splash", that is hit an electrode or leave the coordinate system to the sides. The increased cooling due to the higher gas pressue is clearly evident in the concentration of the ions after 300 μs at about z=320 mm, the potential minimum of the DC potential. The

plot does seem to indicate that there is a difference between "terminal" positions between the two gas pressure configuration in the range between 40-80 mm, which is the position of the first electrodes of the RFQ. Figure 6.6 is a close-up on this region effectively displaying collision events with the electrodes as no "flying" ions can be localized there after 300 μs. Whereas out of 887 Ba ions for a gas pressure of 0.01 Torr 371 ions find their end in these first electrode segments, for a gas pressure of 0.1 Torr the count is reduced to 302 ions. These findings support the hypothesis that even though it seems suprising it is the case that the increased gas pressure provides increased radial confinement even over the first few mm of the RFQ, thereby increasing the "early segment survival rate" of the ions and thus the overall capture efficiency.

Figure 6.7 depicts the ion trajectories at different gas pressures; it can clearly be seen that while a gas pressure of 0.001 $Torr$ is not enough to provide axial confinement (Figure 6.7 (a) and (b)), the substantially higher gas pressure of $P_{Gas} = 0.05$ $Torr$ (Figure 6.7 (c)) damps the radial oscillations quickly and confines the ions efficiently both radially as well as axially.

Again, typical experimental constraints place an upper limit of about 0.01 $Torr$ on the gas pressure [**34**] which is the value adopted in the analysis to follow. Nevertheless, the ability to operate at even higher pressures would be highly beneficial for increased ion confinement.

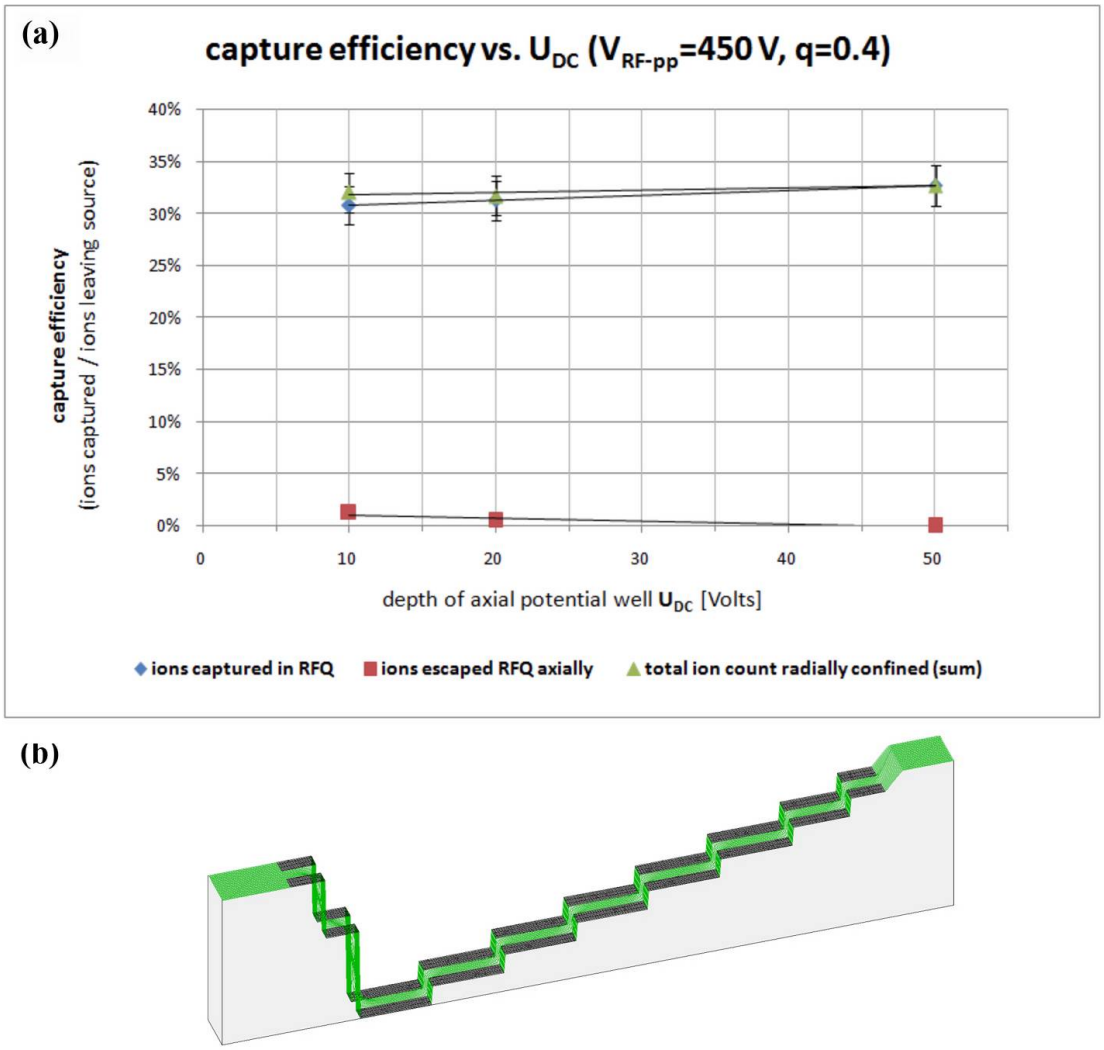

Figure 6.8. (a) Capture efficiency (ions trapped as fraction of ions leaving the source) as function of depth of the axial U_{DC} potential well while holding V_{RF} and ω_{RF} constant such that $V_{RF-pp} = 450$ V and $q = 0.4$ (implying that $\omega_{RF} = 708.6$ kHz). Similarly to the capture efficiency dependence on the gas pressure (Figure 6.4), an increased potential well depth U_{DC} seems to increase the proportion of ions which are trapped of all those ions that enter the RFQ; however it does not seem to significantly increase the number of overall ions that enter and are radially confined. The data-points were obtained with a full SIMION simulation of gas collisions in the RFQ with 887 ions leaving the source per data-point. (b) depicts the $U_{DC} = -20$ V potential well in SIMION's potential energy surface view, the ions enter the RFQ from the right.

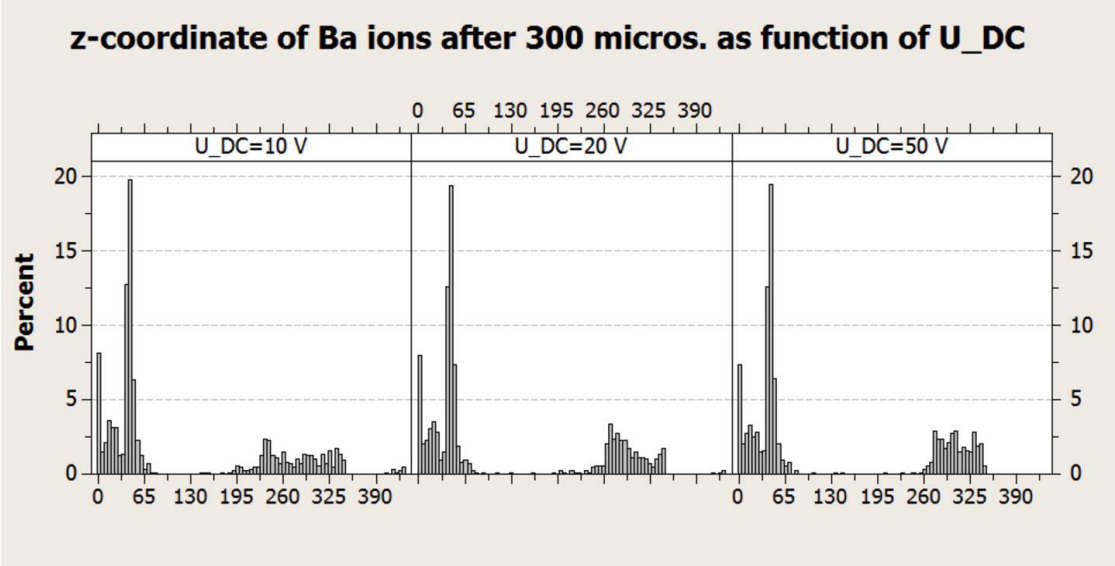

Figure 6.9. "Terminal position" of the Ba ions after 300 μs or upon colliding with the electrodes or the boundaries of the coordinate system. The depth of the DC well seems to have little effect of the fraction of ions that splashes over the first few mm of the RFQ (z = 40-80 mm), contrary to the findings for the gas pressure.

6.4. CE: Depth of axial Potential U_{DC}

The increase in U_{DC} seems to do little to confine additional ions radially (Figure 6.8), contrary to the above results for the gas pressure. The depth of the potential well however does increase the extent to which the ions are axially confined in the minimum of the DC potential well, as can be seen in Figure 6.9. At the same time the deepening of the potential well in the axial direction will provide a divergence term $-\frac{U_{DC}r_0^2}{2z_0^2}$ which counteracts the radial confinement by the given RF field. For the RFQ at hand $r_0 = 9\ mm$ and $z_0 \sim 100\ mm$; thus even for a potential well

depth of $U_{DC} = 50\ V$ this correction amounts only to $\sim 0.2\ V$, negligible compared to the radial potential well depth of $\frac{qV_{RF}}{8} = \frac{0.4*450V}{8} = 22.5\ V$ considered here.

An experimentally-typical higher value for U_{DC} of $20\ V$ is adopted in the further analysis [**34**].

Simulations were also carried in which the position of the source was moved away from the entrance of the RFQ and positioned on an electrode 10 mm away from the opening. Different voltages where then applied to the source electrode to see if the ions could have been "pushed into" the RFQ with greater efficiency than a direct positioning of the source in the entrance of the RFQ could provide. It was found that irrespective of the source voltage moving the source away from the entrance a full 10 mm reduced the capture efficiency in all cases.

CHAPTER 7

SIMION Results: Analysis of RFQ capture Properties for the suggested RFQ Configuration (sRFQc)

So far it was attempted to systematically determine optimal operation parameters for the RFQ within the stipulated experimental constraints (V_{RF}, U_{DC}, gas pressure). The following section shifts the focus of analysis; in the following a determination was made as to what constitutes such optimal operation parameters on the basis of the above analysis to serve as the ground for a more detailed examination of energy and angular capture performance of the RFQ.

Throughout all of the following, the slightly asymmetric U_{DC} potential well shape was used which is indicated in Figure 7.5 (b) on page 66. The DC potential is slightly higher on the "exit" side of the RFQ than on the entrance side which seems to provide more effective axial confinement for the ions leaving the BaF_2 source. The operational parameters are consistently set to the adopted values of $q = 0.4$, $V_{RF-pp} = 450\ V$, $\omega_{RF} = 708.6\ kHz$, $P_{Gas} = 0.01\ Torr$ and will not further be discussed. It is noteworthy that given ω_{RF} and V_{RF-pp} as stated, the associated q for ^{144}Samarium is q_{Sm}=0.38, which is well within the region of stability. The same goes for Fluoride ions with q_F=2.85 (Equation 4.11), too is in the domain

of stability. Thus to differentiate between the ion species the mass determination diagnostics of the CARIBU beamline will be useful.

7.1. sRFQc: Fine-tuning of the Source-Potential U_{source}

In the preceding sections it was concluded that there seemed to be little benefit in positioning the source away from the direct opening of the RFQ. However, it was considered to be an experimental constraint to position the source at least 1.4 mm away from the opening of the RFQ as it needs to be mounted independently on a plate and is not in fact a point source. To fine-tune the capture efficiency the plate potential was varied (Figure 7.1) and it was found that a $U_{source} = 10\ V$ was an effective setting, while capture efficiencies for $U_{source} = 10 - 20$ V are within margins of error of one another. The fact that there does seem to be an increase in capture efficiency over $U_{source} = 0$ V suggests that moving the source back 10 mm from the entrance as tried in the preceding chapter is too far and that an ideal location is closer to the RFQ at a distance of the order of a small fraction of r_0 as was done in this simulation. As the source potential is ramped up to 20 V, Figure 7.1 indicates that the overall capture efficiency seems to diminish slightly as a few of the ions are given enough kinetic energy when leaving the source to escape from the trap axially in the positive z direction.

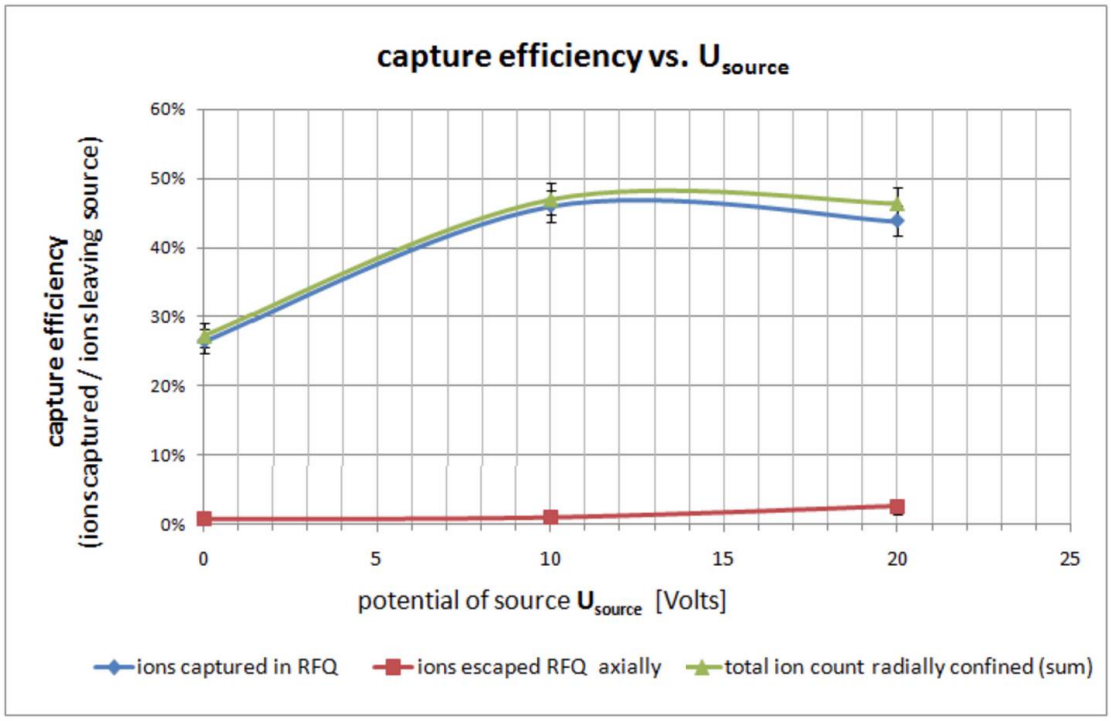

Figure 7.1. The source is positioned on a plate 1.4 mm away from the opening of the RFQ due to experimental constraints. The plate voltage was varied and a 10 V offset towards the baseline voltage of the RFQ was found to be an effective setting in a series of SIMION simulations in which 887 ions were flown each. In accordance with the $U_{DC} = 20\ V$ potential well shape indicated in Figure 7.5 (b) the potential difference towards the first electrode of the RFQ was 12.5 V which accelerated the ions initially.

7.2. sRFQc: CE as Function of the Ion Energy Spectrum

Using all the determined "best" parameters, including $U_{source} = 10\ V$, the SIMION simulation (with 887 Ba Ions flown) suggests an overall capture efficiency of 46.0% ($\pm$2.2%) based on the angular and energy distribution description of the Ba ions which was adopted from the SRIM results for the simulation of the decay

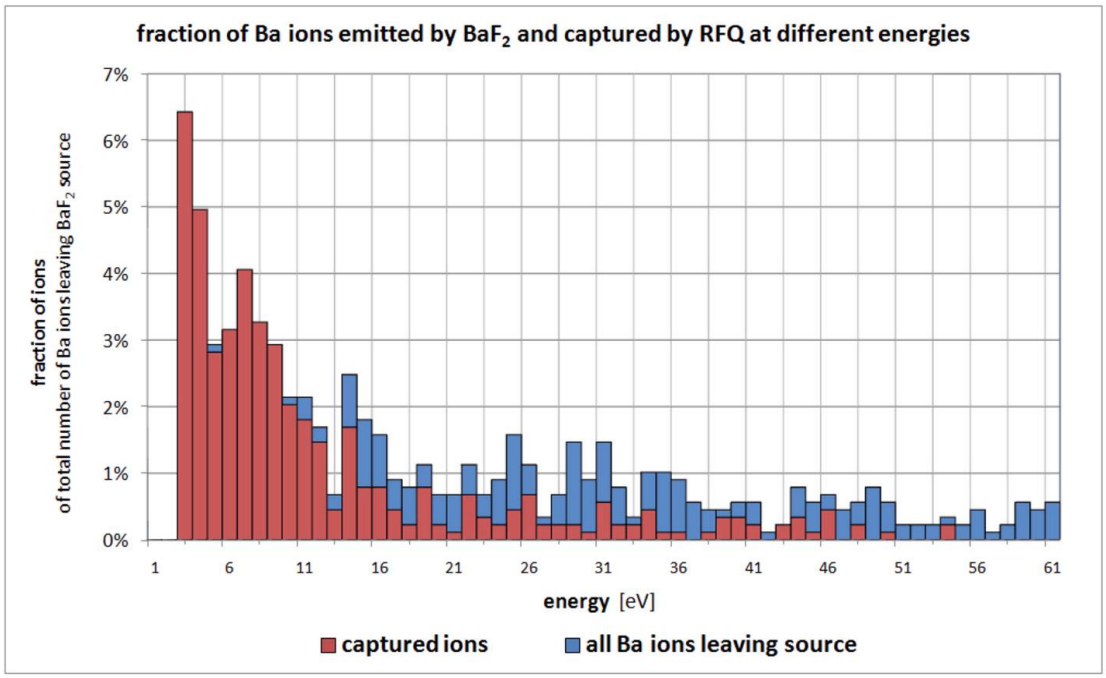

Figure 7.2. Capture efficiency as function of the energy of the Ba ions leaving the BaF_2 source. All values indicate fraction of overall ion count leaving the BaF_2 source. The blue histogram indicates the energy distribution of exiting Ba ions as determined by the SRIM simulation for the source at hand; the red histogram references the exit energies of the Ba ions which were successfully captured at a given energy.

process described for the source at hand. The capture efficiencies as a function of the outgoing Ba energies are depicted in Figure 7.2. It can be seen that the capture efficiency diminishes dramatically for higher outgoing energies for the Barium ions. The median Ba ion energy is 24 eV, and it does seem that the Ba ions which are effectively captured are roughly the ions leaving the source at energies up to the median energy.

To improve the statistics of the data available for the RFQ's capture efficiency as a function of ion energy an alternative ion trajectory configuration was generated which was independent of the energy distribution of the BaF_2 source. It includes eight sets of equal numbers of Ba ions (123) leaving the BaF_2 source at the same energy for every set. The angular distribution in the direction of the normal of the source was adjusted to correspond to the 45 °-peak distribution shown in Figure 3.3 on page 21; the "ϕ"-rotation angle in the XY plane was randomized as explained and indicated in Figure 5.2. Thus the results correspond to the ones in Figure 7.2 except that the capture efficiencies can be given with reasonable accuracy per given Ba ion energy as indicated in Figure 7.3. Up to 25 eV or so the capture efficiency linearly decreases rapidly from very high efficiences for very low energy ions, beyond 60 eV the capture efficiency sinks below 10% and probably vanishes rapidly.

7.3. sRFQc: CE as Function of Ba Ion Angle

With the adjusted ion trajectory configuration used in the preceding subsection the capture efficiency of the RFQ could also be derived as a function of the angle between the Ba ions and the normal to the surface of the source. Figure 7.4 depicts this capture efficiency as a function of the angle bins which average over a non-physical uniform energy distribution between 5 and 60 eV. The results show the trend one would expect, the RFQ favorably captures ions which are released in

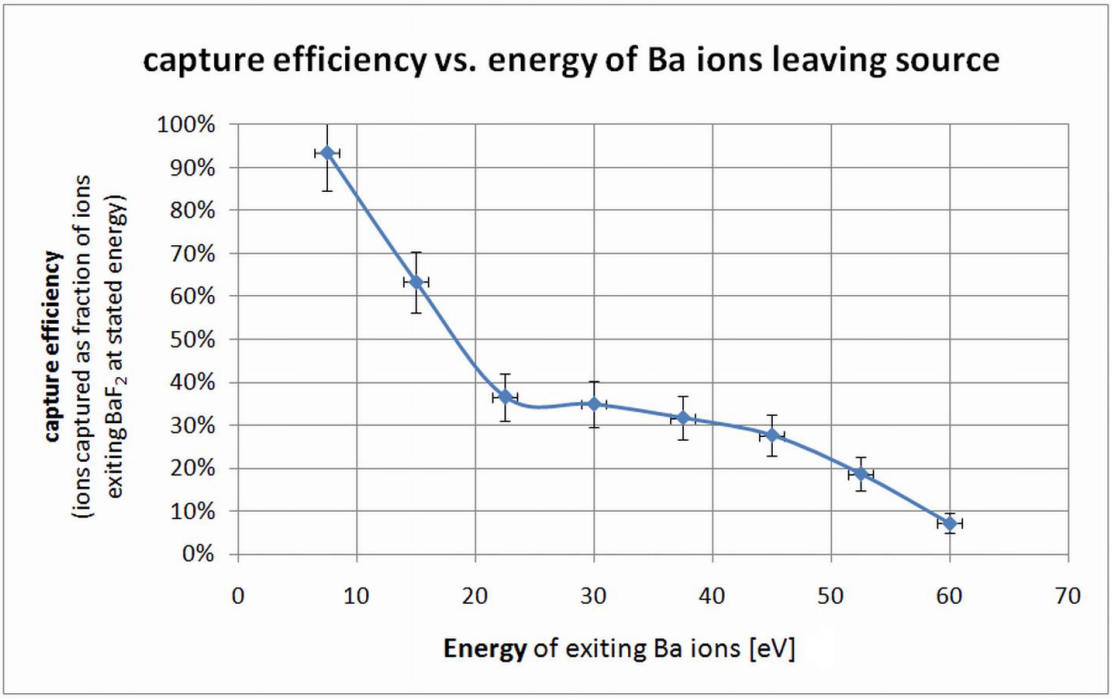

Figure 7.3. Capture efficiency of the RFQ in the suggested configuration as function of Ba ion energy. Every energy bin averages over the angular distribution of exit angles obtained from SRIM for the BaF_2 source (Figure 3.3).

directions mostly parallel to its axis, even though at very low energies almost all ions seem to be captured largely irrespective of their directions.

7.4. sRFQc: Position along the z-Axis of the Trap as Function of Time

Returning to the physical Ba ion trajectory configuration suggested by the SRIM simulation, Figure 7.5 depicts the ion position along the z-axis (axial RFQ direction) as a function of time in the RFQ in the suggested configuration. In 800 μs the standard deviation in ion position along the z-axis is less than 10

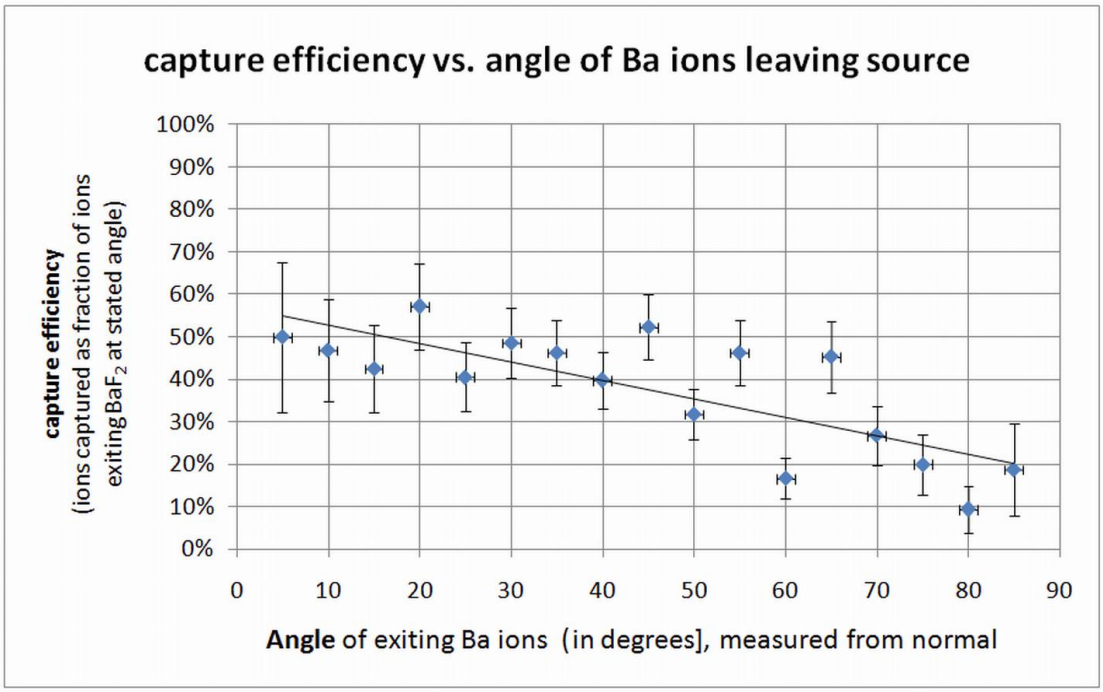

Figure 7.4. Capture efficiency as function of Ba exiting angle. Each angle bin averages over a uniform energy distribution between 5 and 60 eV (Figure 7.3). The magnitude of the stated capture efficiency cannot be compared in magnitude to preceding figures as a different Ba ion energy distribution has been assumed.

mm; the cooling and bunching with the suggested RFQ configuration seems to be quite effective. Figure 7.6 depicts the ion positions after 300 μs in the RFQ for comparison (positions are to scale within the RFQ).

(a)

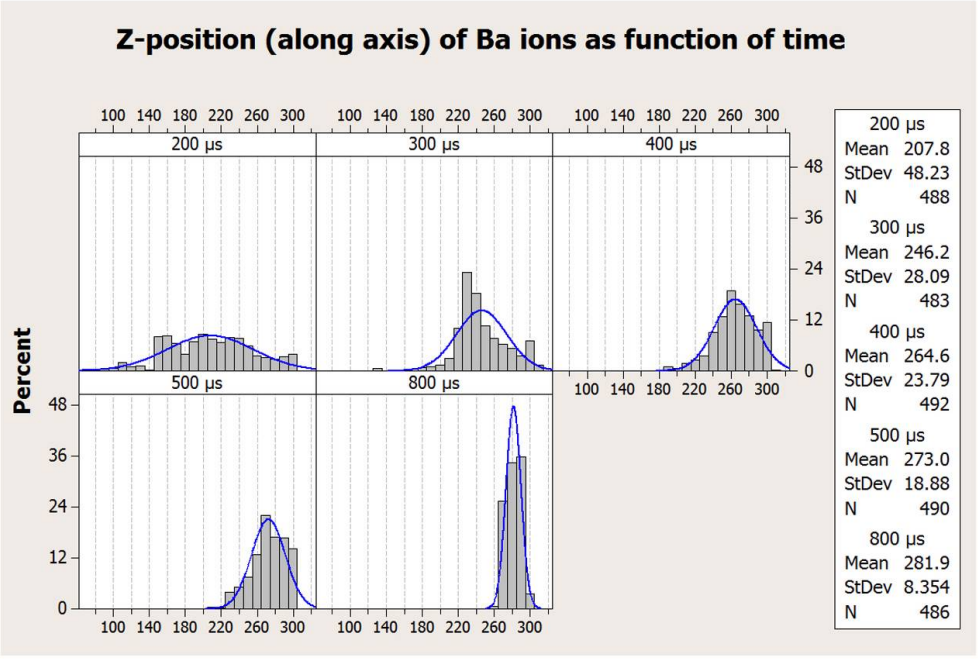

(b)

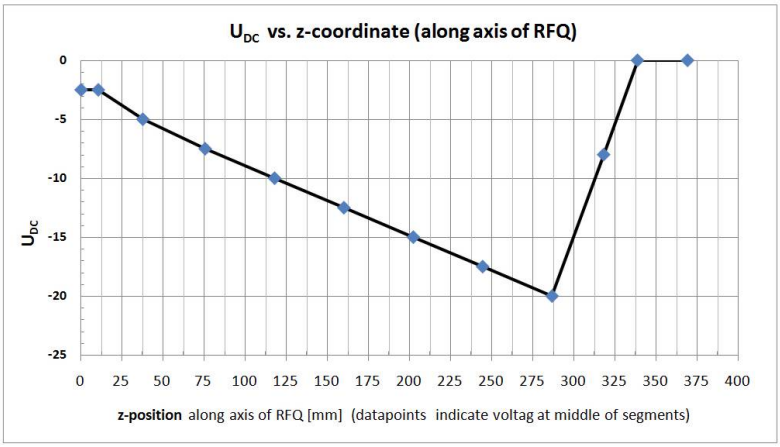

Figure 7.5. (a) Axial (z-position) along the RFQ as function of time given the optimized potential well depicted in (b). Position is given in mm from the entrance of the RFQ. The bunching location seen in (a) seems to correspond clearly to the location of the U_{DC} minimum shown in (b). Figure 7.6 relates the 300 μs ion position to the dimensions of the RFQ as a whole for comparison.

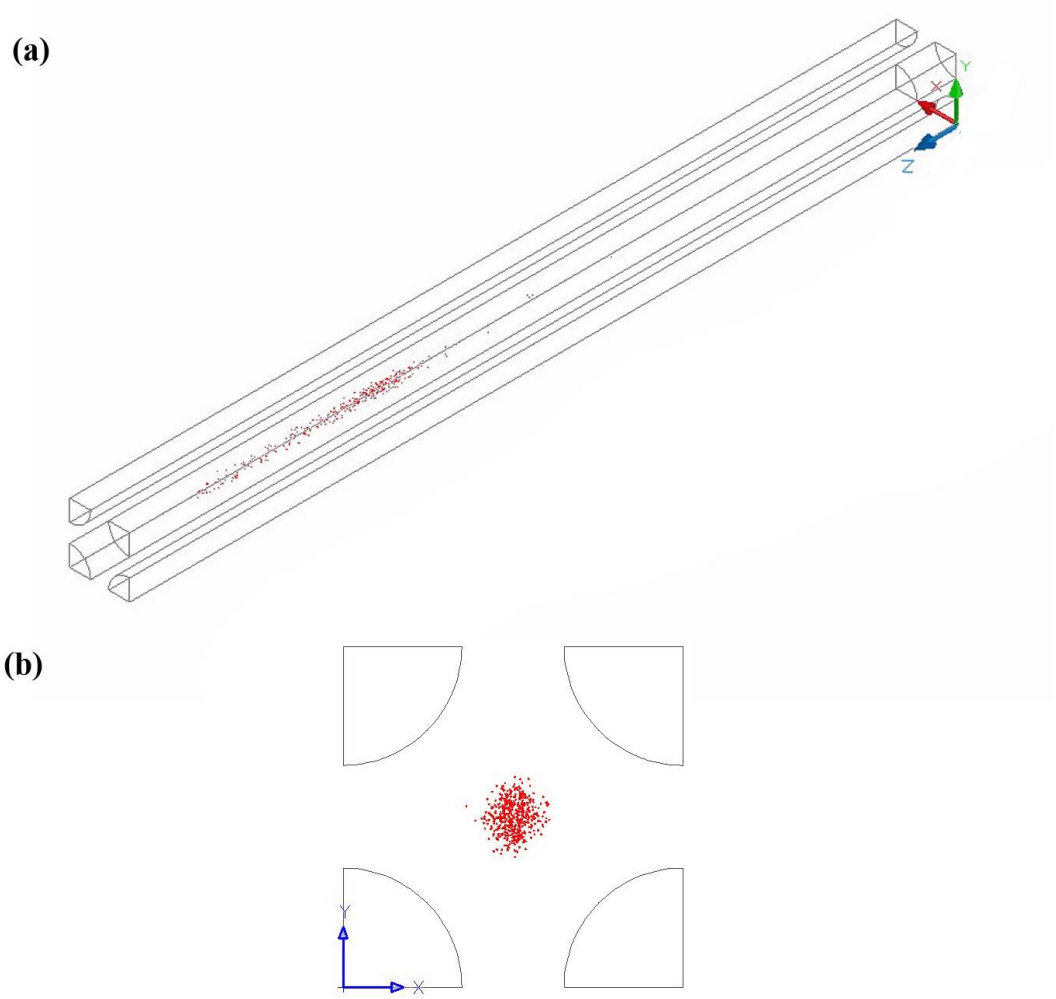

Figure 7.6. (a) Ion positions of 483 Ba ions (captured from 998 ions exiting BaF_2) in the suggested configuration RFQ after 300 μs (in accordance with z-coordinate distribution indicated in Figure 7.5 (a). (b) shows a XY view of ion positions. Positions are to scale within the RFQ; in the construction of the 3D model we were kindly assisted by A. Kambuj, MArch.

CHAPTER 8

Conclusion

It was found through the SRIM and SIMION simulations that it should be possible to capture a substantial fraction of the Ba ions released by the source directly in the RFQ by using RFQ operational parameters which are easily accessible in typical experimental setups. The mean energy of the Ba ions being released has been found to be 305 (±12) eV with a median Ba ion energy of 24 eV. For the suggested RFQ configuration the overall capture efficiency is predicted to be 0.46 (±0.02) Ba ions per incident Sm ion on the BaF_2 layer. Given the radioactivity of the ^{148}Gd used in the source a Ba ion release rate of 23.3 (±1.6) Hz is predicted.

The suggested RFQ configuration parameters are given in Table 8.1. The recommended DC voltages to be applied to every segment of the trap are given in Table 8.2, they account for the 400 Ω resistor chain across the first 8 rod segments where segment one is closest to the entrance (c.f. Figure 9.1).

$\mathbf{V}_{RF-pp}$	$\boldsymbol{\omega}_{RF}$	$\mathbf{p}_{gas}$	$\mathbf{U}_{source}$	distance from RFQ entrance to source
450 V	706.8 kHz	10^{-2} Torr	10 V	1.4 mm

Table 8.1. Suggested RFQ operational parameters.

Segm.i	**1**	**2**	**3**	**4**	**5**	**6**	**7**	**8**	**9**	**10**
$U_{DC(i)}$	-2.5 V	-5 V	-7.5 V	-10 V	-12.5 V	-15 V	-17.5 V	-20 V	-8 V	0 V

Table 8.2. Suggested segment voltages to create -20 V potential well.

The biggest unknown is the charge state of the Barium ions, that is whether they leave the BaF_2 layer singly or doubly charged or with no charge at all. This could not be simulated using a Monte-Carlo approach. The experimental data will shed light on this question, the results presented here can serve as a baseline to compare the experimental results to. Should it be the case that only higher energy Ba ions leave the BaF_2 ionized, changes to the experimental setup might be required considering the fall-off of capture efficiency to essentially zero above 60 eV Ba ion energy. A possible solution could be to capture the Ba ions in a Gas Catcher first, thereby slowing down high-energy ionized Ba ions to the point that they can be trapped in the RFQ with a parameter configuration similar to the one suggested above.

The EXO collaboration is interested in manufacturing a ^{136}Ba source which on average releases one Ba ion for every α-particle recorded by the detector [**13**]. Our SRIM results indicate that such a Ba ejection ratio could be achieved with a BaF_2 thickness of 410 Å ($\pm$10 Å).

CHAPTER 9

Appendix

9.1. RFQ segment length

Please refer to Figure 9.1.

9.2. Automation of the SRIM Workflow: Batch Files

We have developed an automation procedure for SRIM (or more specifically TRIM, SRIM's "Transport of Ions in Matter" module) which builds on automation features already build into SRIM as well as the batch files (let.bat, multilet.bat) which were written by Rebecca Powles, a research scientist in the Applied & Plasma Physics group of the University of Sydney. As our automation system can be seen as another "layer" of automation on top of the ones provided by SRIM and Powles, it is advisable to first be familiar with essentials of their implementations.

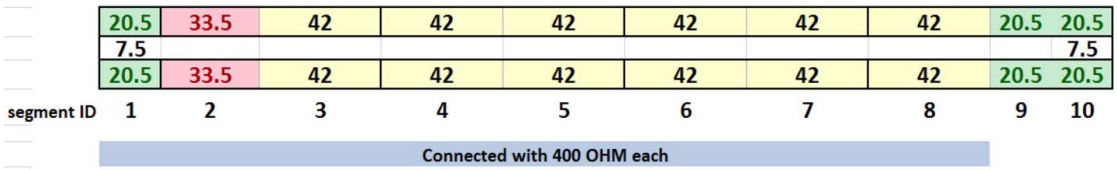

Figure 9.1. Length of the RFQ segments in mm. The entrance of the RFQ is to the left (contrary to the convention used in all other drawings of the RFQ in this thesis). The first 8 segments are connected with a 400 Ω resistor chain.

In the following the essential points of their documentations are reproduced, for further reading references to their documentations are given [**23, 35**]. The relevant documents are also included with the data package provided with this thesis.

Running TRIM automatically (batch mode) [**23**]

TRIM Monte Carlo calculations can be run without any keyboard inputs. This allows TRIM to be run with sequential calculations for a group of related results (sometimes called "running in a batch mode"). Between each run, the input file to TRIM is slightly altered, in order to make similar runs which may be compared. This input file, TRIM.IN, controls the TRIM calculation.

Instructions:

Look at the SRIM file: TRIMAUTO which contains one number.
If the number is 1 then TRIM runs without input, and at completion it saves all datafiles and terminates.
If any other number is in TRIMAUTO, or the file is not present, then TRIM runs normally.

Running TRIM in batch mode:

(1) Run a full TRIM calculation.
(1) Edit the file TRIM.IN, changing any parameters to vary the TRIM calculation.
(2) Run TRIM.EXE by executing it directly.
*(3) When TRIM is completed, save or rename all the *.TXT files*

which have been generated.

(4) Repeat as needed

So essentially to run TRIM in batch mode TRIM has to be set to auto-mode by setting the parameter in the TRIMAUTO file to 1, it needs to be presented with a trim.in file before it is launched, and after the launch the output files have to be recovered from the output directory. This is the exact functionality of the batch scripts written by Powles [REF POWLES]. They will be discussed after introducing the .in files, which serve as the configuration files (not unlike a classical .ini file) for TRIM.

9.3. Adjusting the .in-File

Figure 9.2 shows a trim.in file which saves all the settings necessary to run TRIM and which are entered in the interface shown in Figure 2.2 on page 14. Of particular importance are the following adjustments to the .in-files:

-In Line #3, Ion Number, should be set to a finite number of ions to be calculated (not the default 99999).

- In line #7 to obtain the desired output datafiles (i.e. to have both transrec.txt as well as transmit.txt written to disk) the third number in the row should be set to 3.

-In line #13 to disable the plots and speed up the calculation the Plot Type should be set to 5 (no plots).

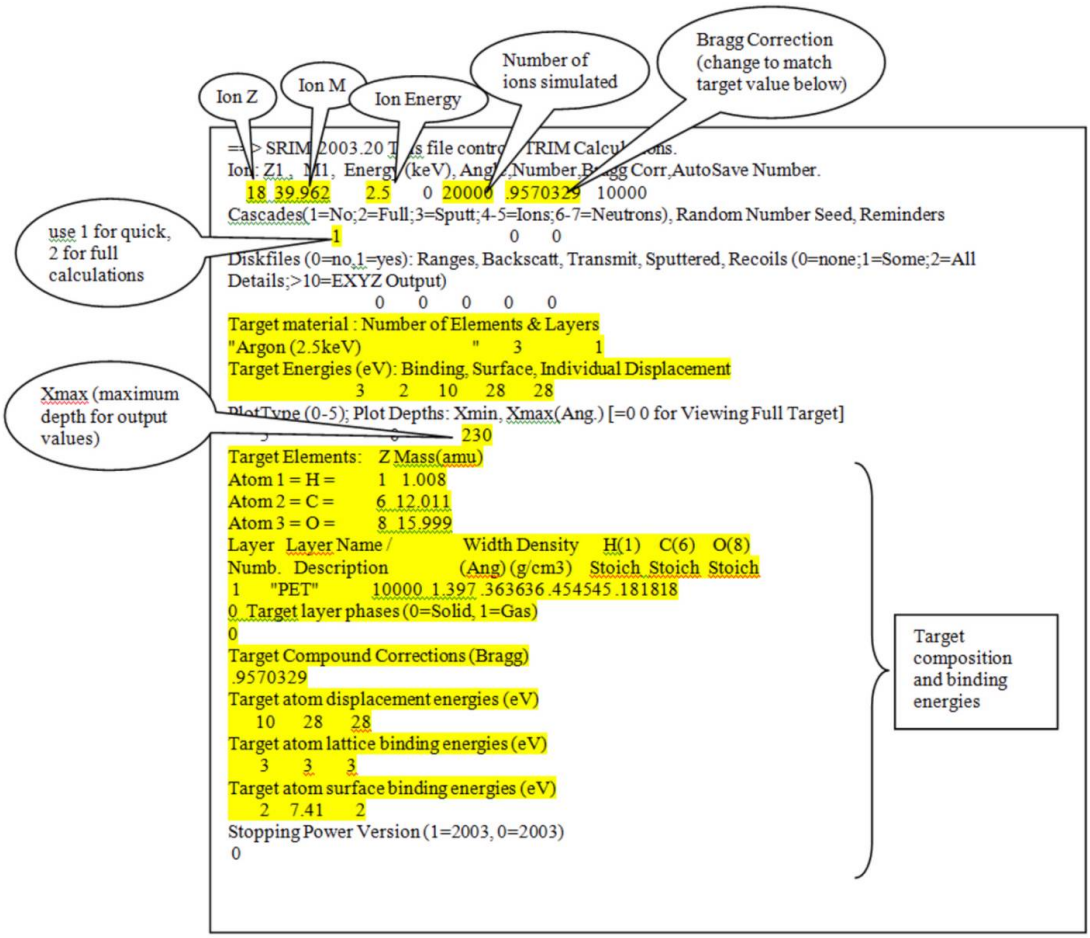

Figure 9.2. A trim.in file. Adopted from [**35**].

Figure 9.3 shows a real life configuration for a .in-file that is suitable to be run in batch mode.

9.4. Adjusting multiple .in-Files and creating a Profile

Further below a method will be presented by which a series of .in-files can be run in batch mode one after the other and their results combined. To give a real life

TRIM.IN

```
==> SRIM-2008.04 This file controls TRIM Calculations.
Ion: Z1 ,  M1,  Energy (keV), Angle,Number,Bragg Corr,AutoSave Number.
    62 143.912     88.5       85     5209        1     1000
Cascades(1=No;2=Full;3=Sputt;4-5=Ions;6-7=Neutrons), Random Number Seed, Reminders
                   2                                      0       0
Diskfiles (0=no,1=yes): Ranges, Backscatt, Transmit, Sputtered, Collisions(1=Ion;2=
                        0       0           3       0               0
Target material : Number of Elements & Layers
"Sm (60) into No. 322 Barium Fluoride    "       2               1
PlotType (0-5); Plot Depths: Xmin, Xmax(Ang.) [=0 0 for Viewing Full Target]
      5                          0             500
Target Elements:    Z   Mass(amu)
Atom 1 = F =         9  18.998
Atom 2 = Ba =       56 135.905
Layer   Layer Name /               Width Density      F(9)  Ba(56)
Numb.   Description                (Ang) (g/cm3)    Stoich  Stoich
1      "No. 322 Barium Fluoride"          500  4.85331 .666667 .333333
0  Target layer phases (0=Solid, 1=Gas)
0
Target Compound Corrections (Bragg)
 1
Individual target atom displacement energies (eV)
     20      25
Individual target atom lattice binding energies (eV)
      3       3
Individual target atom surface binding energies (eV)
      2    1.84
Stopping Power Version (1=2008, 0=2008)
 0
```

Figure 9.3. Real life trim.in configuration as used in the batch runs to create the SRIM data in this thesis.

example consider the following: TRIM per .in-file runs only one angle of incidence on the target. But the Barium source considered in this analysis is isotropic, that is the Sm decay product hits the BaF_2 target from every direction according to the availability of solid angle which scales as $\sin(\theta)$ where the azimuthal angle θ is measured from the normal. So to distribute 2,000 incoming Sm ions according the the availability of solid angle, it would suffice to call TRIM for example nine times,

		SolidAngle Ion count calculator				
sumSinAngles=					SET THIS	
5.74				totalNumberOfIons:	2000	
(auto. Calc.)						
=sin(angle)	=>Percentage	angle in Degrees	SuggestedIonNumbe	=> Suggested .in-file name		
0.09	1.52%	5	30	05TT0030.in		
0.26	4.51%	15	90	15TT0090.in		
0.42	7.37%	25	147	25TT0147.in		
0.57	10.00%	35	200	35TT0200.in		
0.71	12.33%	45	247	45TT0247.in		
0.82	14.28%	55	286	55TT0286.in		
0.91	15.80%	65	316	65TT0316.in		
0.97	16.84%	75	337	75TT0337.in		
1.00	17.36%	85	347	85TT0347.in		

Figure 9.4. Shown is the Excel spreadsheet 'SRIM - SolidAngleCalculator.xls' which is provided as part of the data package. It assigns a given number of ions to nine different angles of incidence and weighs their relative frequencies by the corresponding availability of solid angle.

at angles 5 °, 15 °, 25 °, ... from the normal. The 2000 ions could be split in a way which takes into account the availability of solid angle at that angle of incidence. The results could then be combined to give a dataset that approximates isotropic incidence on the target ions. Figure 9.4 shows an Excel spreadsheet provided with this thesis which does the quick calculation and suggests names for a corresponding set of .in-files; such a set in the following is referred to as "a profile".

Thus a profile would have to be created consisting of nine .in-files named as suggested in the spreadsheet, and then each .in file would have to be adjusted in line three for ion count and angle of incidence accordingly.

Once such a profile for a given total ion count has been written once (i.e. the nine in.-files created which were modified and named accordingly) a global change throughout all the .in-files is relative simple using the "Search and Replace" tool provided in the data package. It allows for a string in all text-coded files within a given folder to be comfortably replaced with another string, thus it is possible to quickly change the target element or ion mass or any other .in-parameter in all .in-files at once. The data package accompanying the thesis contains multiple such solid-angle-adjusted profiles for different total ion counts (500, 1000, 2000, 5000, 30000) which can quickly be adjusted with this method to represent different target or incident ions, etc. The suggested names of the .in-files will be used to streamline the combining of the results of separate .in-file runs into one dataset and will be explained below.

9.5. Powles' MultiLET.bat

Powles provides two batch files, LET.bat and MULTILET.bat, which a) copy a .in file from a set of .in-files (a "profile") into the SRIM directory one at a time; b) launch TRIM and then c) recover the output files and move them into the folder from which the .in file was copied. The following is an excerpt from her documentation; our additions are in bold.

> *I have written two DOS batch files (MultiLET.bat and LET.bat, listings below) which will run SRIM in non-interactive mode on a set of pre-prepared *.IN files, allowing unattended simulation of many*

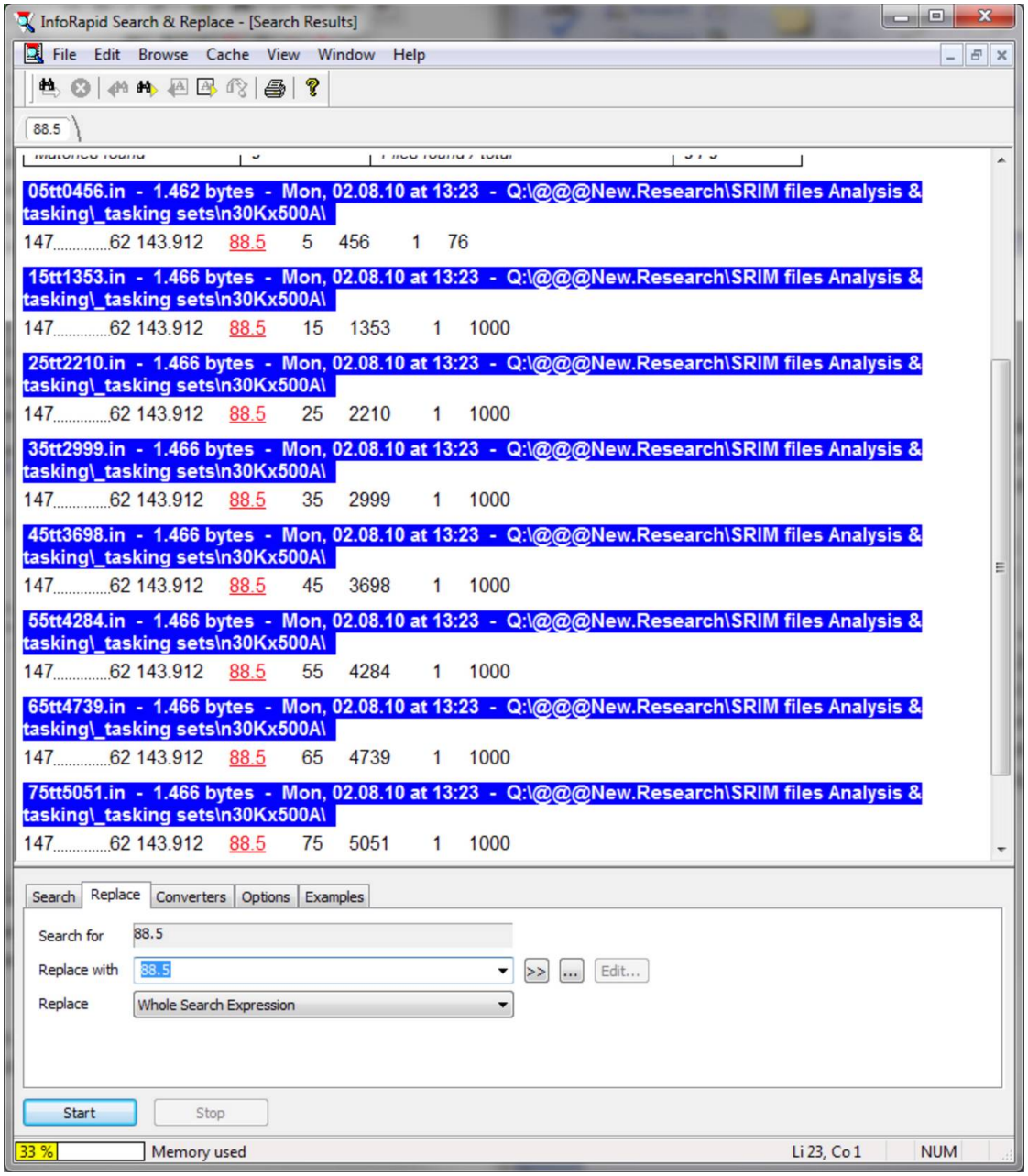

Figure 9.5. InfoRapid Search & Replace allows for the replacing of strings throughout a whole set of text-coded files; it can be used to quickly create copies of solid-angle-adjusted .in-file profiles with altered global parameters such as different incident ion energy.

ion/energy/target combinations. To use these batch files, you need to do the following:

(Note: In this description, the main SRIM directory is the directory where the file TRIM.EXE is located, the data directory is where the input and output files are located).

1. Copy MultiLET.bat and LET.bat to the main directory.

2. Make a new directory ***(profile)*** *which will contain the input and output data for the set of simulations. This is the* ***(profile)*** *directory.*

3. Copy TRIMAUTO (from the main directory) to the data directory. Edit the file so that the first line contains a "1".

4. Make a set of input files (following the format of TRIM.IN), one for each set of conditions you wish to simulate, and save them in the data directory. Make sure these files do not have spaces in their filenames, and that the file extension is .IN

5. At a command prompt, cd to the main directory

6. At the command prompt type: MULTILET.bat ***profiledirectory*** *substituting the pathname of the* ***profile*** *directory. This will run SRIM in non-interactive mode using every *.IN file in the* ***profile*** *directory, moving all output files produced back to the* ***profile*** *directory with names prefixed with the name of the input file.*

*For example, running MultiLET.bat .\myData would run SRIM on all input files with names like *.IN in the* ***profile*** *directory .\myData. If there were two input files .\myData\sim1.IN and \myData\sim2.IN in the* ***profile*** *directory, the output files would be .\myData\sim1_ioniz.txt, .\myData\sim2_ioniz.txt, .\myData\sim1_phonon.txt etc.*

So what is required is a set of .in files (profile) which are put in a directory in the actual SRIM program directory, and then multiLET.bat (which itself is to be stored in the root of the SRIM folder) is to be called with the name of the directory containing the .in files as a parameter.

9.6. Another Layer of Automation: Combining transrec and transmit Files

The multiLET.bat provided by us has been changed from the original state in which Powles provides it. Powles code will copy the .in files one by one into the SRIM directory, set SRIM to load it, start TRIM and then at the end of the run recover the output files and copy them back into the profile folder with the name of corresponding .in file that was responsible for the configuration of the run added as a suffix to the end of it. Then Powles code will go to the next .in file and repeat the procedure once every .in file has been used once by SRIM and its results recovered.

Our additions primarily concern the combination of results for a given profile, more specifically the combination of the transrec.txt and transmit.txt files that

were generated by every .in file. They contain the information of all the ions that have left the target layer in the positive x-direction, that is have either been transmitted (transmit.txt) or knocked out (transrec.txt) by the incoming ions (Note that the recording of these two files has to be turned on in all the .in-files by editing line seven as indicated in Figure 9.3). My additions to multilet will call upon the open source stream editor SED.exe, which is a tool for the command line modification of streams ported from the Linux world (it is provided with the data package in a windows version). In the modified multilet file SED is called to

- Cut off the headers of the transrec.txt and transmit.txt files
- Insert the name of .in file at the beginning of every line of the transrec.txt/transmit.txt

It is for this reason that is was suggested to follow the name convention for the .in files of [angle]TT[ionCount]. In the Excel spreadsheet which will later be generated from the result, this convention will result in the angle of incidence and the ion count for that angle being included as the first 2 columns in the spreadsheet, with all other columns simply being moved to the right.

After all the .in files have run through, the stream editor is called upon to combine all transrec and transmit files into one big file called "AllTransmittedIons_[NameOfProfile]". If angle and ion counts have been altered between the .in files, no information will have been lost in this file compared to the single output files, as the specifics of the .in run have been written into every row of the AllTransmittedIons_[NameOfProfile].txt.

For further processing Excel macros have been provided with data package (in the file "Analysis Macros.xls"), but without documentation. Once the All-TransmittedIons_[NameOfProfile] file has been loaded into Excel, the essential operation is a “text-to-columns” conversion of the content of the spreadsheet which interprets both space " " as well as the capital letter "T" as delimiters of data with the option activated of treating repeated delimiters as one. The macro "SRIM_freshenUpAllTransmittedIons()" will provide this functionality and more.

For some reason SRIM structures the transrec and transmit files slightly differently which is unfortunate when combining the output files into one consolidated file with all ions. However, if the incident ion is not the same as one of the target ions our automation offers a solution which preserves all information. The difference between transrec and transmit is an extra letter “T” that SRIM inserts in the transmit.txt file in every line to indicate that the ion has been “T”ransmitted which offsets all the columns with respect to transrec. However, due to our choice of delimiters the column which simply contains the T in transrec will be deleted, with the effect that the columns again align properly. If one were now interested in the transmitted ions, one would only need to sort or filter the data by the atomic weight column and could thus isolate all ions which have been transmitted.

9.7. The Profile Manager (ProfileManager.bat)

So far we have discussed the automation with one profile, that is with one folder containing a series of .in files which differ with respect to one another in one parameter such as angle of incidence, ion count or something similar.

The profile manager allows for multiple of these profiles to be called upon and it has the added feature of writing all the console output (Figure) that the modified multiLET.bat produces for every profile as a log file into the profile folder. The profilemanager has the very simple content

Multilet2.bat [name of profilefolder1]

Multilet2.bat [name of profilefolder2]

This code calls MultiLET2.bat with the name of the profile folders as a parameter one at a time. MultiLET2 essentially calls our modified MultiLET.bat passing on the profile/folder name, however it does so in a way that writes the console output of that MultiLET operation into a log file in the profile folder. This comes in very handy with long unattended runs, as one can quickly check if SRIM or one of the batch files ran into any problems – as indicated for example by "file not found" errors upon multilet's attempt to copy the output from the SRIM output folder into the profile folder.

As an indication of performance, with a BaF_2 thickness of 50 nm and incident Sm ions at about 100 keV, it took TRIM and the ProfileManager about 6.5 hours to process a 50,000 incident ion dataset on a Core 2 Duo 2.6 GHz Intel CPU.

ap_console.txt

```
working in data directory: n30Kx500A
**********************************************
*** processing the following input files:******
**********************************************
 Directory of Q:\@@@New.Research\SRIM\n30Kx500A

08/02/2010  01:23 PM             1,462 05TT0456.in
08/02/2010  01:23 PM             1,466 15TT1353.in
08/02/2010  01:23 PM             1,466 25TT2210.in
08/02/2010  01:23 PM             1,466 35TT2999.in
08/02/2010  01:23 PM             1,466 45TT3698.in
08/02/2010  01:23 PM             1,466 55TT4284.in
08/02/2010  01:23 PM             1,466 65TT4739.in
08/02/2010  01:23 PM             1,466 75TT5051.in
08/02/2010  01:23 PM             1,466 85TT5209.in
               9 File(s)         13,190 bytes
               0 Dir(s)  158,873,169,920 bytes free
**********************************************
*************** STARTING THE LOOP *************
data directory: n30Kx500A
processing 05TT0456
copied input file 05TT0456.in to main directory as TRIM.IN
finished running TRIM
results in: n30Kx500A\transrec_05TT0456.txt
results in: n30Kx500A\transmit_05TT0456.txt
generating new xtrans* files, cutting off headers...
...done. this seems to work generally, as long as sed.exe is in same folder.
***********DONE WITH THIS TRIM.IN iteration ******************

****** this was the last TRIM.IN // NOW: doing final file operations (xtrans*

xtransrec_05TT0456.txt
        1 file(s) copied.
xtransmit_05TT0456.txt
        1 file(s) copied.
transrec.txt
transmit.txt
        1 file(s) copied.

...done good sir.
```

Figure 9.6. Example of console output generated by the modified MultiLET which is written into the profile folder as a [ProfileName]_log.txt file by the ProfileManager.

9.8. SRIM Automation Code

The files are provided with further documentation in the data package submitted with the thesis.

9.8.1. ProfileManager.bat

REM call multilet2 with the name of the profile for every profile=folder.

REM e.g. the file is in C:\SRIM and there is a c:\SRIM\500x500A folder with a few .in files

REM then call with ==> call multilet2.bat 500x500A

REM good luck.

call MULTILET2.bat n30Kx500A

9.8.2. MultiLET2.bat

call Multilet.bat %1 >%1\%1_ log.txt

REM this passes on the call with directory to multilet and makes sure its outputs are written to logfile in that directory.

9.8.3. MultiLET.bat

@echo off

REM call this batch with 2 paramaters: relative data-directory which should be the profile name (%1)

*REM for each input file in the data directory *.IN*

REM run LET.BAT to process the file in TRIM and move the output

REM pass data directory as first argument

REM pass profile name as second argument for naming of final output files

echo working in data directory: %1

echo.

*echo *********************************

*echo *** processing the following input files:******

*echo *********************************

dir %1.IN*

dir %1.IN >CON*

REM the second con line makes sure that it gets shown on the screen even though we are writing to log file.

*echo ***********************

echo.

echo switching to batch mode in TRIM

echo by moving trimauto from the batch folder into the main folder...

echo if file not found just below don't worry.

echo ...it just means there was no trimauto in the data directory.

move %1\trimauto >nul

echo.

*echo *************** STARTING THE LOOP *************

echo.

REM this loops through all the trim.in's

FOR %%a in (%1.IN) do call:PROC_FILE %1 %%a*

cd %1

*@echo *********************************

```
@echo ********************************
@echo ****** this was the last TRIM.IN // NOW: doing final file operations (xtrans*, AllTransmittedIons.txt...)*****
@echo ******************************
@echo.
copy xtransrec* transrec.txt
copy xtransmit* transmit.txt
copy transrec.txt+transmit.txt AllTransmittedIons_%1.txt...
cd..
@echo.
@echo ...done good sir.
echo.
rem this avoids final dummy run!
GOTO :EOF
:PROC_FILE
@echo data directory: %1
@echo processing %~n2
REM no longer needed as goto EOF was inserted above. that way more elegant.
REM if "%~n2"=="" (ECHO *** FINAL DUMMY RUN DETECTED, EXIT I WILL GOOD SIR ***)
REM if "%~n2"=="" (GOTO :EOF)
call let.bat %1 %~n2
```

REM echo on

REM inserting angles into text file

@echo generating new xtrans files, cutting off headers...*

sed "s/^/%~n2 /" <%1\transrec_%~n2.txt>%1\xtransrec_%~n2.txt

sed "s/^/%~n2 /" <%1\transmit_%~n2.txt>%1\xtransmit_%~n2.txt

REM delete the initial info headers in both types of files

sed -i -e "1,7d" %1\xtransrec_%~n2.txt

sed -i -e "1,2d" %1\xtransmit_%~n2.txt

@echo ...done. this seems to work generally, as long as sed.exe is in same folder.

@echo.

*@echo ********** DONE WITH THIS TRIM.IN iteration *******

@echo *** done with this %~n2 *** >CON*

@echo.

GOTO :EOF

Bibliography

[1] Audi, G., Wapstra, A.H., Thibault, C., "The Ame2003 atomic mass evaluation (II)" *Nuclear Physics,* A729 p. 337-676, December 22, 2003

[2] G. Savard et al., "Studies of neutron-rich isotopes with the CPT mass spectrometer and the CARIBU project", International Journal of Mass Spectrometry 251: 2-3, (2006)

[3] L. J. Kaufman, "Searching for Double Beta Decay with the Enriched Xenon Observatory", 2010 J. Phys.: Conf. Ser. 203 012067

[4] H.V. Klapdor-Kleingrothaus, A. Dietz, H. L. Harney, and I.V. Krivosheina, "Evidence for neutrinoless double beta decay", Modern Physics Letters A 16: 37, 2409-2420 (2001)

[5] H.V. Klapdor-Kleingrothaus, A. Dietz, and I.V. Krivosheina, "Neutrinoless Double Beta Decay: Status of Evidence", Foundations of Physics 32: 8 (2002)

[6] H.V. Klapdor-Kleingrothaus, I.V. Krivosheina, A. Dietz, and O. Chkvorets, "Neutrinoless double beta decay with enriched 76Ge in Gran Sasso 1990-2003", Physics Letters B 586 pp. 198-212 (2004)

[7] H.V. Klapdor-Kleingrothaus, and I.V. Krivosheina, "The evidence for the observation of $0\upsilon\beta\beta$ decay: The identification of $0\upsilon\beta\beta$ events from the full spectra", Modern Physics Letters A 21: 20 pp.1547-1566 (2006)

[8] C. Arnaboldi et al., "First results on neutrinoless double beta decay of 130Te with the calorimetric CUORICINO experiment", Physics Letters B, Volume 584, Issues 3-4, 1 April 2004, Pages 260-268

[9] C. Arnaboldi et al., "Physics potential and prospects for the CUORICINO and CUORE experiments", Astroparticle Physics, Volume 20, Issue 2, November 2003, Pages 91-110

[10] D.S. Leonard et al., "Systematic study of trace radioactive impurities in candidate construction materials for EXO-200", Nuclear Instruments and Methods in Physics Research A 591 pp.490-509 (2008)

[11] David R. Lide, and Norman E. Holden, "Section 11, Table of the Isotopes". CRC Handbook of Chemistry and Physics, 85th Edition" 2005, Boca Raton, CRC Press, Florida

[12] N.D. Scielzo et al., "Double-β-decay Q values of 130Te, 128Te, and 120Te", Phys. Rev. C 80: 2 (2009)

[13] M. M. Díez, "Single ion sources in arbitrary media", presented at SMI-10, International Workshop on Stopping and Manipulation of Ions, Stanford University, March 21-24, 2010 (http://smi-10.stanford.edu/smi-10/talks/EXOSourcesSMI10.pdf)

[14] YR Yen, "Single atom barium sources for EXO barium tagging development", Bulletin of the American Physical Society, APS April Meeting 2010, Vol. 55, No. 1

[15] S. Slutsky, "Overview and Status of the EXO-200 Double Beta Decay", Bulletin of the American Physical Society, APS April Meeting 2010, Vol. 55, No. 1

[16] P.J. Mohr, B.N. Taylor, D.B. Newell, CODATA Recommended Values of the Fundamental Physical Constants: 2006, National Institute of Standards and Technology

[17] Nubase2003 evaluation of nuclear and decay properties, Nuclear Physics A, 2003, vol. 729, page 3-128

[18] Gratta G., "EXO - an overview", Bulletin of the American Physical Society, Volume 54, Number 10, 3rd Joint Meeting of the APS Division of Nuclear Physics and the Physical Society of Japan (2009)

[19] M. Laval et al., "Barium fluoride - Inorganic scintillator for subnanosecond timing", Centre d'Études Nucléires de Grenoble, LETI/MCTE, 85 X, 38041, Grenoble Cedex, France

[20] J. F. Ziegler, J.P. Biersack, U. Littmark, "The Stopping and Range of Ions in Solids", 1985, Pergamon Press, New York

[21] K. Wittmaack, Reliability of a popular simulation code for predicting sputtering yields of solids and ranges of low-energy ions", Journal of Applied Physics, Vol. 96, Number 5, Sept/1

[22] J. F. Ziegler, J.P. Biersack, U. Littmark, "The Stopping and Range of Ions in Solids - Accuracy Data" (http://www.srim.org/SRIM/SRIM2008.htm)

[23] J.F. Ziegler, "TRIM - Setup and Input", 2010 (www.srim.org/SRIM/SRIM%2008.pdf)

[24] J. F. Ziegler and J. M. Manoyan, "The Stopping of Ions in Compounds" Nuclear Instruments and Methods, Vol. B35, 215-228 (1989)

[25] N. McLachlan, "Theory and Application of Mathieu Functions", 1964, Dover Publications

[26] M. Abramowitz, I. Stegun, "Handbook of mathematical functions", 1972, Dover Publications

[27] J. Wodin, "Single Ion Trapping in a Buffer Gas and Liquid Xe Energy Resolution Studies for the EXO Experiment", Dissertation, Stanford University (2007)

[28] W. Paul, "Electromagnetic traps for charged and neutral particles", *Nobel Lecture*, 1989

[29] F. Herfurth et al., "A linear radiofrequency ion trap for accumulation, bunching and emittance improvement of radioactive ion beams", Nuclear Instruments and Methods in Physics Research Section A, Volume 469, Issue 2, 11 August 2001, Pages 254-275

[30] J.V.F. Vaz, "Precision Mass Measurements of Selected Isotopes of Platinum", PhD Dissertation, University of Winnipeg, 2002

[31] E.A. Mason and H.W.Schamp, "Mobility of gaseous ions in weak electric fields", Ann. Phys., New York 4 (1958), pp. 233–270

[32] D. Dahl, "SIMION For the personal computer in reflection", International Journal of Mass Spectrometry 200: 3, Dahl, D. (2000)

[33] D. J. Manura, "SIMION 8.0 user manual", Scientific Instrument Services, Inc., Idaho National Laboratory, (2006)

[34] Private communication with Prof. G. Savard, Argonne National Laboratories/Department of Physics, University of Chicago

[35] R. Powles, "Notes_on_SRIM.doc", Applied & Plasma Group, University of Sydney, 2010 (http://www.physics.usyd.edu.au/~powles/SRIM_batchmode/SRIM_batchrunning.html)